Horizon 2020
European Union funding
for Research & Innovation

ITS4LAND
innovations for
land tenure

Deliverable 4.2

Data quality assessment of UAV-based products for land tenure recording

31st May 2018

Version 1.0

Abstract:

Technical report and manual on key flight scenarios for land tenure recording in East Africa including main impact factors on final product quality.

Project Number: 687828
Work Package: 4
Lead: University of Twente
Type: DEM

Dissemination: Public
Delivery Date: 31st May 2018
Contributors: Claudia Stöcker, Mile Koeva, Francesco Nex

Peer reviewed by: Cornelia Schmidt, Tarek Zein

The its4land consortium consists of the following partners:

University of Twente (UT)
KU Leuven (KUL)
Westfaelische Wilhelms-Universitaet Muenster (WWU)
Hansa Luftbild AG (HL)
Institut d'Enseignement Supérieur de Ruhengeri (INES)
Bahir Dar University (BDU)
Technical University of Kenya (TUK)
Esri Rwanda (ESRI).

Executive Summary

This deliverable encompasses a technical report and manual on key flight scenarios for land tenure recording in East Africa based on main impact factors on final product quality. Based on a literature review, three main quality metrics – namely accuracy, reliability and completeness – were extracted to assess the fitness-of-use and data quality. More than 40 datasets from 8 UAV field campaigns were used to demonstrate the correltation of the final quality of the data products with the quality metrics. Reliability is primarily affected by the image quality which in turn is mainly determined by the sensor characteristics. However, also flying mode and spatial resolution impact the quality and quantity of information that can be extracted from UAV images. Accuracy refers to a crucial metric when it comes to the assessment of data products for land tenure recording as many jurisdictions impose a threshold for the maximum tolerable geometric accuracy of surveyed parcel boundaries. Different ground reference point setups were evaluated. High-grade onboard IMU and GNSS equipment are highly beneficial to achieve geometric accuracies below 5cm while reducing the need for ground measurements. Completeness is mainly affected by external parameters such as land cover, terrain and wind.

The manual on key scenarios assigns four specific scenarios according to spatial scale and geometric accuracy. User requirements are set by possible use cases in the its4land target countries. Insights of product specifications (i.e., orthomosaics) are gained from the analysis of influencing internal and external parameters on the reliability, accuracy and completeness. The four different scenarios are defined in such a way that the specifications meet the user requirements which ultimately implicates a sound data quality.

Keywords: Fit-for-purpose, UAV, photogrammetry, data quality assessment, geometric accuracy

Contents

Table of Figures

1. Introduction

Sub-Saharan African countries have an immense challenge to map millions of unrecognized land rights in the region. Land administration systems, the technologies, and processes that maintain information about the relationship of people to land are recognized as a crucial tool to achieve sustainable economies, environments, and social cohesion: land tenure recording helps to deliver tenure security, dispute reduction, investment opportunities, and contributes to good governance. Seeking for sustainable development, the four land administration functions – namely land tenure, land value, land use and land development - are facilitated by appropriate land information infrastructures. These ideally combine cadastral and topographic datasets to link the built environment (including legal and social land rights) with the natural environment (including topographical, environmental, and natural resource information) (Enemark 2004). Therefore, land information and geospatial data serve as reliable base data and thus are crucial to the successful implementation of land policies and strategies. Existing literature proves that spatial data collection is *the* key challenge of an effective land administration system (Bennett & Alemie 2015; Zevenbergen et al. 2013). Establishing and maintaining the spatial database is the most expensive and time-consuming but also most essential tasks in land administration.

its4land aims to deliver an innovative suite of land tenure recording tools that respond to Sub-Saharan Africa's immense challenge to rapidly and cheaply map millions of unrecognized land rights in the region. its4land is a European Commission Horizon 2020 project funded under its Industrial Leadership program, specifically the 'Leadership in enabling and industrial technologies – Information and Communication Technologies ICT (H2020-EU.2.1.1.)', under the call H2020-ICT-2015. ICT innovation is intended to play a crucial role. Many existing ICT-based approaches to land tenure recording in the region have not been highly successful: disputes abound, investment is impeded, and the communities poorest lose out. its4land seeks to reinforce strategic collaboration between the EU and East Africa via a scalable and transferable ICT solution. Established local, national, and international partnerships seek to drive the project results beyond research and design (R&D) into the commercial realm. its4land combines an innovation process with emerging geospatial technologies, including smart sketchmaps, UAVs, automated feature extraction, and geocloud services, to deliver land recording services that are end-user responsive, market-driven, and fit-for-purpose. The transdisciplinary work also develops supportive models for governance, capacity development, and business capitalization.

The advent of low cost, reliable, user-friendly and lightweight Drones / Unmanned Aerial Vehicles (UAVs) and recent developments in digital photogrammetry and structure from motion (SfM) image processing software solutions have created new opportunities to obtain nadir and oblique aerial imagery. Due to their flexible operational setups, UAVs can bridge the gap between time-consuming but high accurate field surveys and the fast pace of conventional aerial surveys. The basic mapping workflow (see Fig. 1) starts with a data acquisition flight with a mounted camera. In most cases, the camera takes vertical images during the UAV flight at predefined waypoints or at a given time interval. Data products include high resolutions two-dimensional orthorectified maps (orthomosaic), terrain models (digital surface models and digital terrain models) and 3D models (point clouds and mesh).

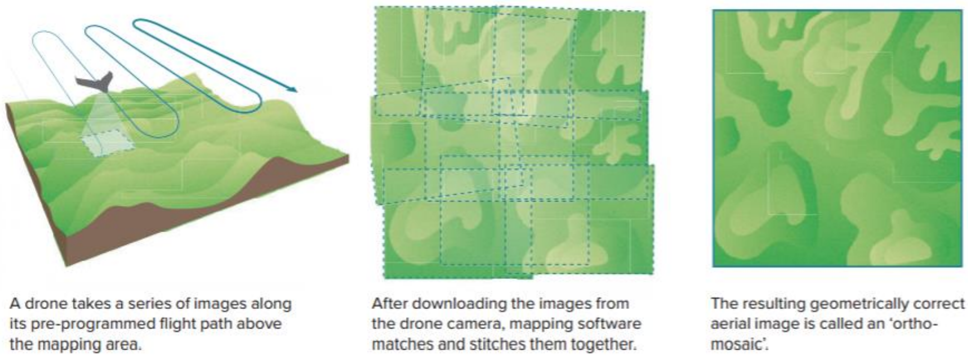

Figure 1: UAV mapping workflow, Source: FSD report 2016 (http://drones.fsd.ch)

Orthomosaics are especially valuable because they provide the base for cadastral mapping and further visual interpretation, manual digitization (Devriendt & Bonne 2014; Barnes & Volkmann 2015), automatic mapping or feature detection procedures (Crommelinck et al. 2017). Besides the benefits of the increased speed of boundary delineation using aerial images (Ali et al. 2012; Lemmen & Zevenbergen 2009), the notion of 'what-you-see-is-what-you-get-properties' (Enemark et al. 2014) has largely reduced the number of mistakes during boundary demarcation and land adjudication. Additionally, the visual representation of an orthomosaic facilitates land right holders to verify the spatial extent of their property on the land right certificate (Enemark et al. 2014). However, the fact that UAV-derived geographical information can support decision-making processes involving people's Rights, Responsibilities, and Restrictions (RRRs), ultimately raises questions about the quality of respective data and parameters that influence the data quality. (Grant 2017) is saying: "[…] while "everyman/everywoman" can own or operate a drone, not everyone is an expert on the quality of data that drones provide." Thus, this report outlines a sound overview of relevant data quality metrics and how various internal and external parameters influence the final product quality. The results will enable end-users to make decisions how and to which extend UAVs can be used in order to provide reliable, accurate and complete orthomosaics which can support land tenure data acquisition.

This report is structured as the follows. Section two provides a short overview of data quality concepts that create the basis for the selection of appropriate quality metrics. The third section describes the data collection and UAV field campaigns carried out for the its4land project. An in-depth analysis of influencing parameters is outlined in section four. This analysis will help define key flight scenarios for land tenure recording as concluded in section five.

2. Data quality of UAV-based orthomosaics – what is relevant for land tenure recording?

2.1 Concepts of data quality

Data quality is a multi-dimensional concept (Pipino et al. 2002; Devillers et al. 2002) and refers to the condition of data. More concrete, ISO 8402 defines quality as the “totality of characteristics of a product that bear on its ability to satisfy stated or implied needs” and thus expounds the fitness to serve the purpose of the data in a given context. In this regard, (ISO 2013) depicts a comprehensive framework of data quality concepts for geographic information (Fig.2). The framework includes both perspectives: the data producer who can use the quality evaluation to reflect upon the product specification and the data user who can assess the data quality if it satisfies his/her predefined requirements. Following this, data quality reports are only valid against the user requirements or the product specifications being set. This report will include both perspectives.

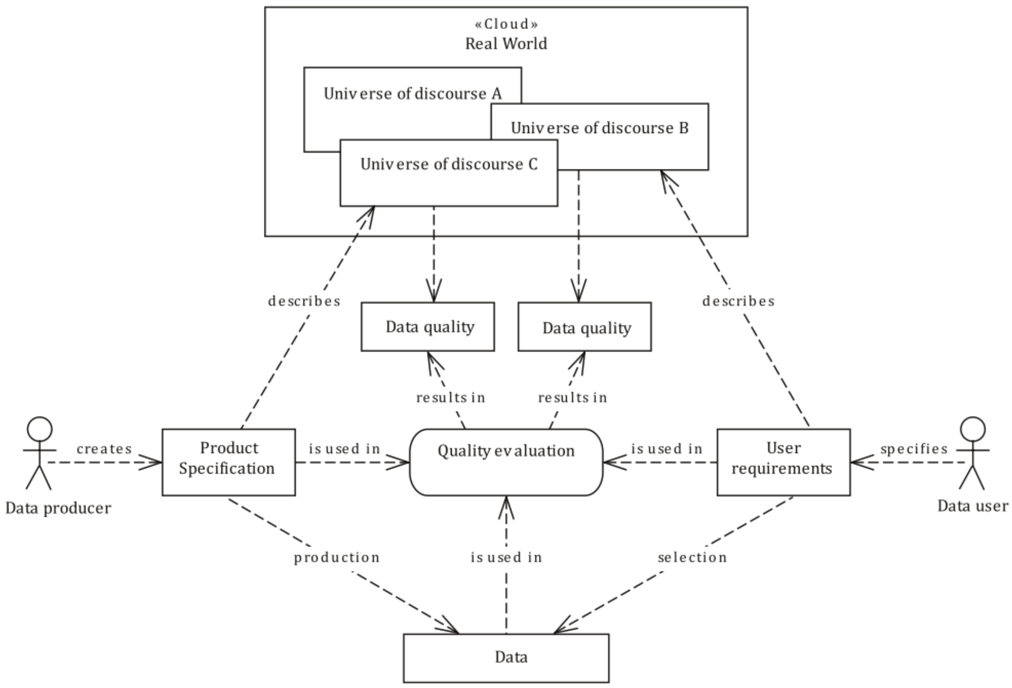

Figure 2: Framework of data quality concepts (ISO 2013)

Data quality elements allow for the evaluation of how well a dataset meets the criteria outlined in its data product specification or user requirements. Following (Pipino et al. 2002) quality evaluation can be both: task-independent or task-dependent. Here, task-independent metrics reflect the condition of the data outside its context and thus can be applied to any dataset. In contrast, task-dependent metrics refer to the organization’s business rules, company and government regulations, and constraints provided by the database administrator. These are only valid for a particular application/context (Pipino et al. 2002). As the analysis is in the context of land tenure recordation, all metrics will be task-dependent.

What characterizes good data quality in the context of UAV-derived products for land tenure recording? Which metrics need to be addressed in a quality assessment framework? Table 1 outlines three different approaches which build the short-list for the selection of relevant data quality metrics.

1) The first approach by (Pipino et al. 2002) specifies different data quality dimensions and can be applied to any data and thus remains very generic.
2) (ISO 2013) outlines five different data quality elements to evaluate the quality of geographic data.
3) (Rahmatizadeh et al. 2018) propose a set of parameters to select a fit-for-purpose data collection method in land administration. The parameters are differentiated according to the data collection process, post collection parameters, and the data parameters. The definition of those parameters is based on a Delphi study among land administration experts. As the derived parameters aim to measure the fitness of use, they can also be seen as data quality metrics.

Table 1: Overview of different data quality metrics

Data quality dimensions (Pipino et al. 2002)	Standardized data quality measures for geographic information (ISO 2013)	Influential parameters in the choice of a fit-for-purpose data collection method in land administration (Rahmatizadeh et al. 2018)
Accessibility	Completeness	Accuracy
Appropriate amount of Data	Logical consistency	Open and transparent procedure
Believability	Positional accuracy	Compliance with common standards
Completeness	Temporal quality	Data update mechanism
Concise Representation	Thematic accuracy	Sharing data mechanism
Consistent Representation		Verifiability
Ease of Manipulation		Reliability
Free-of-Error		Upgradeability
Interpretability		Ease of implementation
Objectivity		Affordability
Relevancy		Metadata
Reputation		Time efficiency
Security		Repeatability
Timeliness		Completeness
Understandability		
Value-added		

2.2 Data quality metrics for UAV-based orthomosaics for land tenure recording

The selection of relevant metrics is key to a sound data quality evaluation. As this work solely focuses on UAV-based orthomosaics as base data for further definition of the spatial extent of RRR, only metrics that assess the dataset as such were considered. Following (Rahmatizadeh 2018), this encompasses **completeness**, **accuracy, and reliability** (Fig. 3). Here, completeness is defined as the extent to which data is correctly reconstructed and is not missing. This metric coincides among all three approaches shown in Table 1. Accuracy refers to a specific metric for the evaluation of geospatial data and is a crucial aspect of judging the fitness of use for land administration applications as each jurisdiction sets its own tolerable geometric accuracy value in the delineation of boundaries. Here, (ISO 2013) defines the positional accuracy as "closeness of gridded data spatial position values to values accepted as or being true". Regarding UAV-based orthomosaics, reliability might be interpreted as the representation of the real world. Although reliability itself is not explicitly outlined by the other concepts, the two metrics "free-of-error" and "believability" by (Pipino et al. 2002) are very similar. As the data is not assigned with semantics and does not include thematic information, logical consistency and thematic accuracy as additionally listed by (ISO 2013) is not applicable for this analysis.

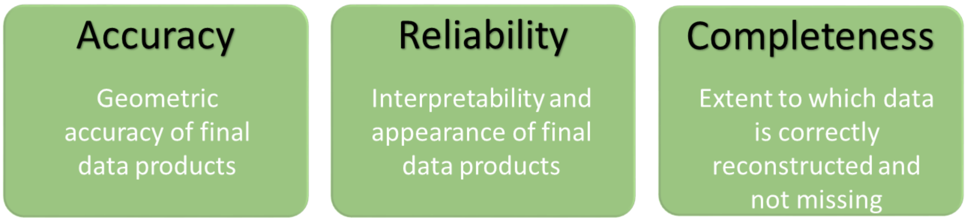

Figure 3: Data quality metrics for evaluation of UAV-based orthomosaics for land tenure recording

A high number of scientific output that deals with quality of UAV-based products for many different purposes has been published already. Some of these papers have compared UAV-based data acquisition to other techniques such as GNSS surveying, aerial mapping or terrestrial laser scanning (Toth & Jóźków 2016; Colomina & Molina 2014; Eltner et al. 2015). Others have assessed the residuals on ground control points (GCPs) and check points from their performed flights with different image configurations (Agüera-Vega et al. 2016; Rehak et al. 2013; Gerke & Przybilla 2016; James et al. 2017). Most of these papers discuss the influence of a single parameter on the final quality using controlled test flights to evaluate different goals. However, practitioners cannot always afford to wait for perfect flying conditions and many UAV flights occur in non-perfect environments due to temporarily restricted flight permissions, staff availability, product delivery deadlines, weather amongst others. Here, various parameters are interconnected and influence the final quality of UAV-derived orthomosaics. Thus, this report includes a systematic analysis of different parameters using more than 40 datasets from 8 UAV field campaigns to correlate the final quality of the data product with different parametersetups.

3. Data material for quality evaluation

Most of the UAV flights carried out for the its4land project are used for the data quality evaluation. The list encompasses controlled test flights in Germany and Tanzania (Zanzibar) where different parameter configurations were tested. Additionally, its4land UAV flights in Rwanda and Kenya are included in the systematic analysis as well.

3.1 Data acquisition

Germany

The UAV field campaigns in Europe included many test flights to firstly demonstrate different UAVs and secondly assess the flight performance of the DT18 PPK, the UAV which was acquired for the its4land project. Various sensor settings and different GCP setups were evaluated to obtain recommendations for the African partners. Two out of six datasets are suitable to be added to the systematic analysis in this report. The remaining datasets were either very focused on a small area (test data with Ebee RTK and albris of sensefly), or evaluated the sensor settings or were carried out in poor meteorological conditions (light snow cover or very cloudy) which do not allow to draw general conclusions and recommendations.

The first dataset includes the demo flight of the GerMAP G180 in June 2016 (Fig. 4). The licensed UAV operator company GerMAP carried out the flights in the rural area of Amtsveen in North Rhine-Westphalia/Germany. The GR180 is a modular UAV which can carry various payloads. Before the flight was carried out, 13 ground reference points were evenly distributed over the area of interest. The points were measured using the Leica GS14 GPS receiver in Real Time Kinematik (RTK) mode. A final measurement accuracy of less than 2cm was achieved. The flight planning was done with the open source software Mission Planner and forward overlap and side lap were determined with 80% and 65%, respectively. Flying height was set to 190m, leading to a ground resolution of 5cm. During the flight, the UAV followed the predefined trajectory and captured images during a specified time interval. However, the take-off and landing were completed in manual mode which requires a high experienced and well-trained UAV pilot.

Figure 4: UAV data acquisition in Germany (GerMAP)

The second dataset includes a UAV flight campaign using the DT18 PPK equipped with the APX-15 GNSS-Inertial board. With an extent of 1.4 km^{2}, the test site surrounds the monastery “Benediktinerabtei Gerleve” which is located close to Coesfeld in North Rhine-Westphalia/Germany. The site is characterized by a slightly undulated terrain with an altitude range from 140m to 200m ASL (above surface level). A large part of the site can be categorized as agricultural land area. Field data collection encompassed the UAV airborne data acquisition and RTK-GNSS based measurements of 22 ground reference points. More than 2500 images were captured to cover the whole study area. The camera was triggered by a predefined time interval of 1.5 sec which corresponds to 80% forward overlap at a cruising speed of 16 m/s. To ensure a stable image block and reliable photogrammetric processing, the side lap was set to 70%. The flight was performed in a constant height of 100m above surface level and a regular flight pattern leading to a ground sampling distance (GSD) of 2.8cm.

Following the recommendations for slightly undulated terrain by (Gerke & Przybilla 2016) a cross flight was completed at the end of the data acquisition. For several processing scenarios, data-logs of the APX-15 were post-processed with Applanix POSPac UAV software. Correction data was provided by 1sec interval RINEX data of a virtually created reference station located in the center of the test area. The maximal baseline between the UAV platform and the virtual reference station was 650m.

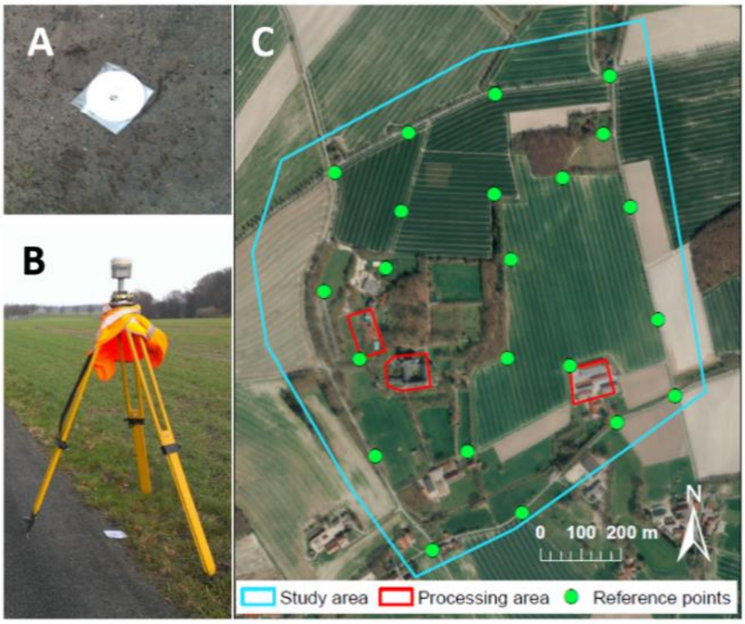

Figure 5: Ground reference points. A: shape, B: means of measurement, C: distribution of reference points and selected processing areas for point-to-plane comparison

As illustrated in Figure 5, ground reference points were marked with white painted circles with a diameter of 12cm. They were evenly distributed over the area of interest and fixed with special surveying pegs. The center of each reference point was measured with a GNSS receiver in RTK mode achieving an accuracy of 2cm. A summary of the equipment being used in Germany is outlined in Table 2.

Table 2: Overview of equipment for UAV flights in Germany

Name	GerMAP G180 (GerMAP)	DT18 PPK (Delair Tech)
		
Type	Fixed-wing UAV	Fixed-wing UAV
Sensor	Ricoh GR 18.3	DT18 3Bands PPK
Area	Amtsveen (209 ha) – 2 flights	Gerleve (140 ha) – 1 flight
Date	June 2016	March 2017
GCP	13 points with Leica GS14	22 points with Leica GS14

Rwanda

In April 2016, the Ministerial Regulations N°01/MOS/Trans/016 relating to UAVs were officially gazetted (RCAA 2016). As outlined in Deliverable 4.1, regulations are very prescriptive and contain subparts dealing with UAV registration and marking, privacy and safety, airworthiness certification, operating rules, and pilot licensing. Before any commencement of any flight activities, the UAV needs to be registered and marked with a unique identifier. Furthermore, pilots, as well as the operating organisations, need to hold specific licenses issued by the Rwanda Civil Aviation Authority. These requirements demand a high standard of UAV professionality and make it a challenge for new companies and institutions to obtain legal flight permissions. Rwanda distinguishes between certified UAV pilots, registered UAV, accredited UAV operators, and flight/activity permits. Since the beginning of the its4land project, INES-Ruhengeri, Esri Rwanda, and ITC are in the process to obtain all necessary documents and clearance for the start of their own UAV flights. Following a specific UAV training by the manufacturer DelairTech in October 2016 in Toulouse, the colleagues from Esri Rwanda and INES-Ruhengeri became certified UAV pilots in the UK in November 2017. However, the procedure to formally accept this pilot license in Rwanda has not yet been completed, but would be a pre-requisite for INES-Ruhengeri to become a certified drone operator for research and education. Thus, the itsl4and consortium closely collaborates with the first UAV certified company in Rwanda: Charis UAS Ltd., which operated and piloted all UAV flights which were carried out for the its4land project in Rwanda.

Figure 6: UAV data collection in Rwanda

Together with Charis UAS its4land successfully commenced the maiden flight of the DT18 in Rwanda in January 2018 (Fig. 6). Additional data collection activities were carried out in the designated research area in Musanze District. Both, peri-urban as well as urban areas were captured with UAV images. As shown in Table 3, the data acquisition flights were carried out with four different UAVs; two rotary-wing UAV (Inspire 2, 3DR Iris+), one hybrid UAV (FireFLY6) and the fixed-wing UAV (DT18 PPK) which was purchased for the its4land project. Type and sensor specifications are presented in Table 3. The 3DR Iris+ can be categorized as a low-cost UAV whereas Inspire2 from DJI refers to a semi-professional UAV with a focus on filmmaking. Both, the FireFLY6 and the DT18 PPK are survey-grade UAVs of which the FireFLY6 presents a low cost solution, and the DT18 PPK refers to a professional UAV with high-end components.

Table 3: Overview equipment for UAV flights in Rwanda

Name	InspirePro (DJI)	3DR Iris+
		
Type	Rotary wing UAV	Rotary wing UAV
Sensor	Zenmuse X5S	Canon Power SX 260 HS
Area	Busogo (50 ha) – 2 flights	Busogo (7 ha) – 4 flights
Date	January 2018	March and April 2017
GCP	19 points with Leica CS 10	16 points with Trimble GeoXH
Name	FireFLY6 (BIRDSEYEVIEW)	DT18 PPK (Delair Tech)

		
Type	Hybrid UAV	Fixed-wing UAV
Sensor	SONY A6000	DT18 3Bands PPK
Area	Muhoza (94 ha) – 2 flights	Gahanga (14 ha) – 1 flight
Date	January 2018	January 2018
GCP	29 points with Leica CS 10 and Trimble GeoXH	14 points with Trimble GeoXH

The FireFLY6 collected data of an urban environment in Mushoza Sector, whereas the InspirePro was flown over a peri-urban area in Busogo Sector. Due to the regulatory restrictions and the difficulty to find sufficient large landing sites, the DT18 PPK maiden flight was conducted from a cricket stadium 20 km south of the City of Kigali. The current visula line of sight rules of 300m only allowed to capture images over a cricket stadium embedded in a rural area in Gahanga Sector. Both, the InspirePro and the FireFLY6 were equipped with a consumer-grade GNSS antenna which allows geotagging of all images. However, resulting geometric accuracy is limited to a few meters making the measurements of additional GCPs indispensable. Artificial ground reference points were marked and measured with the help of INES-Ruhengeri and Esri Rwanda to include known point coordinates for georeferencing as well as for quality control. The ground reference points that were used have a quadratic shape with an edge length of 30cm showing a black and white chess pattern (cf. Fig.7). Points were measured with two different GNSS devices. The first was a Leica CS10 set as base and rover with a final RTK measurement accuracy of less than 2cm. The second device was a handheld Trimble GeoXH which received RTK corrections via the Rwanda CORS GeoNet which allowed for final measurement accuracies of 10cm.

Figure 7: Measurement of ground reference points in Rwanda

Kenya

By the end of January 2018, the Technical University of Kenya (TUK) received a special flight permission for the UAV data collection activities with the DT18 for the its4land project. After a lengthy application procedure which took more than one year, the special permission was granted by KCAA and was valid from 18.02. to 09.03.2018. Next to the formal permission, it was also necessary to inform administrative representatives at the county level to ensure that the mission can be conducted without any complications.

The area of interest was defined by the case site where the Work Package 3 conducted its mapping activities for Smart Sketch Maps since the UAV orthomosaic will serve as the base data. The site is situated in the rural area of Kajiado between the villages Ngatatoek and Mailua. The focus during the UAV flights in Kenya was put on areal coverage rather than test flights over one particular area. Reconnaissance was conducted on the first day to familiarize with the working environment, get to know the locals, locate the paths and to identify the most appropriate locations within the area of interest to allocate a suitable landing site and set up new reference points. The new control points were established using standard iron pins. Access to the most suitable landing site was problematic as the river could not be passed with vehicles. Thus, all UAV and GNSS equipment had to be carried by foot to the area of interest. At this study site, only the DT18 PPK UAV was utilized to capture all data (Figure 8 and Table 4). During four individual overlapping flights, a total area of 330ha was covered with images having a ground resolution of 5 cm.

Figure 8: Initial calibration and update of the software in Kenya

Table 4: Overview equipment for UAV flights in Kenya

Name	DT18 PPK
	
Type	Fixed-wing UAV
Sensor	DT18 3Bands PPK
Area	Mailua (332.3 ha) – 4 flights
Date	March 2018
GCP	7 points with Spectra Precision SP80

GNSS measurements were conducted by the surveying company OAKAR services in Kenya. This local surveying company also acts as a member of the valorization panel of its4land and showed a high interest in our data collection activities. Static and RTK survey methodologies were used to transfer/densify the reference / control points inisde the area. During the densification process, two Spectra Precision (SP80) dual frequency geodetic receivers were used to track the satellites simultaneously. In the rapid static survey method, a GNSS SP80 receiver was placed as a base station on a known survey control point, to broadcast the position correction signals to a mobile/roving GNSS SP60 unit to locate the position of the existing control points. Due to unstable weather conditions, it was only possible to establish and measure seven ground reference points instead of 12 as initially planned.

Zanzibar

The UAV flights in Zanzibar were conducted within the framework of a strategic collaboration between the its4land project and the World Bank Group. The project consortium took the opportunity to link with the World Bank funded Zanzibar mapping initiative (ZMI) which collected UAV data of both islands of Zanzibar: Unguja and Pemba. Together with local stakeholders such as the World Bank representative, the regional manager from SenseFly, We Robotics flying Labs Tanzania as well as key persons from the Commission of Lands and the State University of Zanzibar multiple UAV test flights were conducted with the local UAV equipment (Fig. 9). Here, an Ebee Plus was deployed with a base station for PPK corrections (Table 5). By the time the flight were carried out in February 2018, no UAV regulations were in place for Tanzania or Zanzibar in particular. However, the local police and respective authorities were notified beforehand in order to avoid public concerns and to allow a smooth data acquisition. All test flights were carried out over a peri-urban area in the central part of Unguja. Different flight parameters such as flying height, image overlap, and flight patterns were chosen to evaluate the impact on the final data quality.

Figure 9: UAV data collection with We Robotics Flying Labs in Tanzania

Table 5: Overview of equipment used for UAV flights in Zanzibar

Name	Ebee plus PPK (SenseFly)
	
Type	Rotary wing UAV
Sensor	S.O.D.A camera
Area	Kibonde Muzungu (15 ha) – 6 flights
Date	February 2018
GCP	11 points with Stonex S9 III

Before the flights were carried out, 11 ground reference points were evenly distributed over the area of interest. They were measured using a Sokkia S9 III GNSS device in RTK mode. Thus, a final measurement accuracy of less than 2 cm could be achieved. However, all measurements were completed in terms of the local datum Arc1960. Due to missing correct transformation parameters, all coordinates were corrected using mean offset values which were measured with the dataset containing the highest resolution (1.5cm) and the largest image overlap (70% forward and 70% side lap). Transformation parameters used were -4.1906m in X and -7.3315m in Y direction.

3.2 Data processing

The aerial images acquired by UAVs cannot be immediately used as a map. However, by applying the photogrammetric methodology this can achieved. Photogrammetry is the science of using 2D image measurements to extract 3D information about the position and the geometry of an object. In photogrammetry two images, also called stereo-pair, are acquired from two different positions in space and share an overlapping area which allows the visualization of the same objects depicted in each of the stereo image. The photogrammetric workflow allows images to be processed into a cartographic map. The workflow can be divided into three main steps: (i) image orientation, (ii) dense point cloud extraction and (iii) orthophoto generation.

The determination of image orientation comprises both: interior orientation and exterior orientation parameters. Interior orientation elements include principle point offset, sensor size, pixel size, focal length, and distortion parameters of the camera. Parameters of the exterior orientation are defined by the position of the camera (X, Y, Z) and the attitude (yaw, pitch, roll) when the image was taken. In contrast to known interior orientation parameter of metric cameras - as often used for traditional aerial photography -, low-cost and consumer-grade cameras - mainly equipped in UAVs - are considered to be non-metric since the internal orientation parameter change with any flight mission. Thus, the interior orientation parameters need to be estimated during a camera calibration procedure which is mostly achieved with a simultaneous self-calibration.

After the interior orientation is determined, the second step in the image orientation process is to establish the relation between image space and object space. This process is accomplished by determining the camera position and attitude in the object space reference system. As these parameters refer to the image position in relation to a coordinate system, the transformation from object space coordinates to absolute coordinates is crucial. The exterior orientation of an image is defined by six parameters: the 3D position of the projection center in terms of the ground coordinate system and the three rotation angles (the attitude). To obtain relevant information two main approaches can be distinguished: direct and indirect georeferencing (Fig. 10).

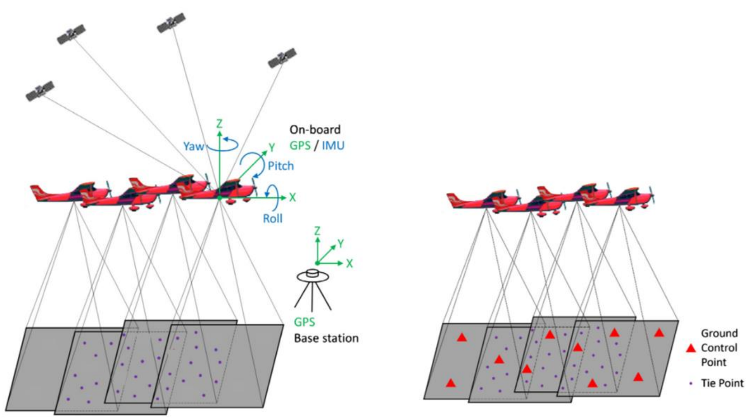

Figure 10: Direct (left) versus indirect (right) georeferencing, modified according to (Toth and Jóźków, 2016)

Indirect georeferencing is achieved by measuring ground control points visible in the aerial images which would then allow the transformation of relative orientation to absolute orientation. Here, GCPs and checkpoints should be established in the field. Since GCPs need to be measured in image space, size and color should be chosen according to visibility and signalization conditions. A minimum of three GCPs are treated as weighted observations during the least-square bundle block adjustment, either one-stage or two-staged. Here, the one-stage optimization is considered to be the most rigorous (Nex & Remondino 2014).

In direct georeferencing the coordinates of camera exposure positions (exterior orientation parameters) are used directly to define the absolute spatial framework for image processing. For this, either single frequency GNSS data acquired from geo-taggers attached to the camera or on-board IMU and GNSS devices log the position of each exposure. Here, (Jóźków & Toth 2014) outline that low-grade positioning devices are unable to improve the quality of UAV mapping products. However, today the integration of airborne dual frequency GPS receivers and/or real-time-kinematic (RTK) or post-processing kinematic (PPK) on-board devices open new options for direct georeferencing. In contrast to the sole use of code-based observations, RTK provides carrier-phase measurements that promise absolute accuracy in sub-cm range (Gerke & Przybilla 2016). To facilitate the real-time estimation of positional coordinates and attitude parameters, a permanent radio-link from the UAV to the ground control station is obligatory. (Gerke & Przybilla 2016) showed that RTK corrected geo-tag information of the L1 GNSS receiver deliver results that can compete with residual accuracies which are obtained with the indirect georeferencing procedure. In contrast to RTK, PPK systems do not require a permanent radio link to the ground control station. Here, the positional accuracy of the geo-tag is enhanced during the image post-processing using GNSS observation from a continuously operating reference system (CORS) or a GPS base station. Figure 11 defines the decision tree which can be followed according to the technical equipment at hand.

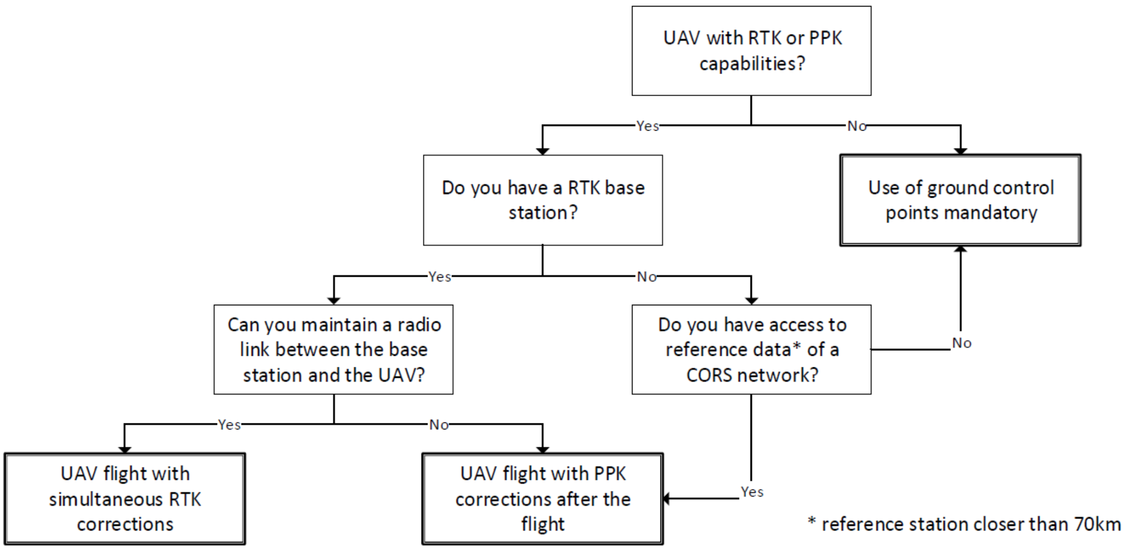

Figure 11: Options to achieve high level geometric accuracies

The orientation of the block of aerial images (also called aerial triangulation) is computed by different methods, such as the bundle block adjustment which orients a block of images and follows the mathematical model of the collinearity equations (cf. Kraus 2007). For each photo, the bundle of rays (image point, projection center, ground point) can be modeled. Further, all the rays from the different photos that are generated from the same ground point should intersect at one point. By this, all the orientation parameters per image and all the unknown ground coordinates are determined simultaneously.

The term dense image matching refers to matching techniques which aim for a maximum of image correspondences – in the ideal case for each pixel in a reference image a corresponding pixel in the stereo model is found (if no occlusions hamper the matching). The forward intersection of all those points will lead to a dense point cloud in object space. Without having the prerequisites of the intrinsic and extrinsic parameters, the computer vision community developed a fully automatic 3D reconstruction workflow which is known as structure from motion (SfM) (based on Ullman, 1976). Here, the initial reconstruction of the scene geometry is based on the identification and matching of homologous image points (keypoints) in overlapping photos captured from multiple viewpoints. SIFT (Scale-invariant-feature-transformation algorithm) (Lowe 1999) and SURF (Speeded up robust feature algorithm) (Bay et al. 2008) are the most prominent automatic feature-description-and-detection algorithms. Features detected by these algorithms are robust to scale, rotation, and changes in illumination and perspective. At this, interior and exterior camera parameters are simultaneously estimated during this computation step (Remondino & Pizzo 2012). Based on corresponding 3D information of matched image points in an arbitrary coordinate system, the sparse point cloud is densified. Recent state-of-the-art dense matching algorithms embrace semi-global matching (Hirschmüller 2005) and patch-based multi-view stereopsis (Furukawa & Ponce 2010). In conclusion, SfM allows for a fully automatic computation of large image datasets with strong network geometries. However, compared to the conventional photogrammetry, the SfM workflow is mainly criticized for lacking in absolute accuracy (Rosnell & Honkavaara 2012), reliability and repeatability/precision (Colomina and Molina, 2014). Therefore, some software packages take advantages of both approaches – the fast and automatic computation of an initial scene geometry reconstruction and photogrammetric bundle adjustments for rigorous compensation of final residuals. Final data products of image processing workflows include dense point clouds (3D point coordinates) digital surface models (2.5D raster) and orthoimages (2D raster).

For the data analysis in the its4land project, all images were processed using Pix4D mapper Pro (see Fig.12) as it also provides the possibility to modify the parameters and their weights. This option can be highly beneficial to guide sub-processes such as the image orientation and dense point cloud generation phases. The full feature keypoints scale with original image size was chosen to give an accurate result of the tie points. The calibration process was set to standard (if not mentioned otherwise), to ensure the camera external and internal parameters are also optimized.

Ground reference points that were distributed and measured before the commencement of the UAV flight are either used as GCP (weighted observation for georeferencing) or independent check point (quality control). Information about the specific processing characteristics and the number of GCPs and check points are outlined in the appendix of this document.

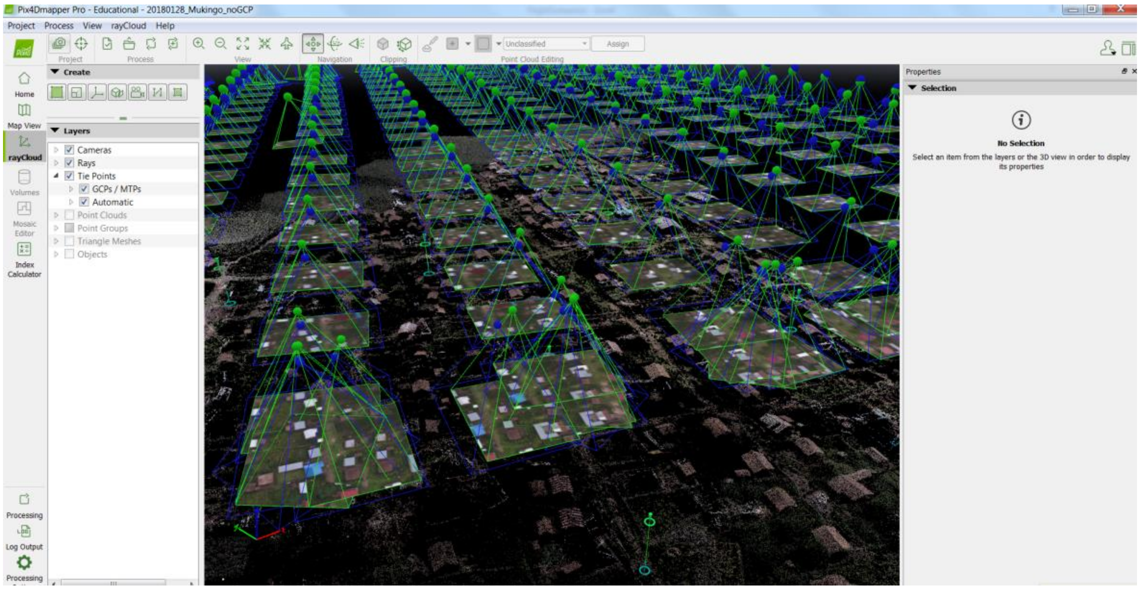

Figure 12: Graphical user interface of Pix4D photogrammetric software

4. Evaluation of data quality

This section includes a systematic analysis of all relevant parameters that are associated with the quality metrics *Reliability*, *Accuracy*, and *Completeness*. Sensor specifications, the type of UAV and flying height refer to important parameters that determine the image quality. As images are the raw data for the photogrammetric processing, they are considered as the smallest entity. By this, the image quality ultimately affects the accuracy as well as the completeness (cf. Fig. 13). In addition to the image quality, accuracy is mainly determined by on-board positioning devices, the configuration of ground truthing strategies, and the way how individual images are captured. The scope of completeness as a data quality metric refers to the entire dataset and particularly to the spatial coverage and alignment of various orthomosaics of different UAV flights.

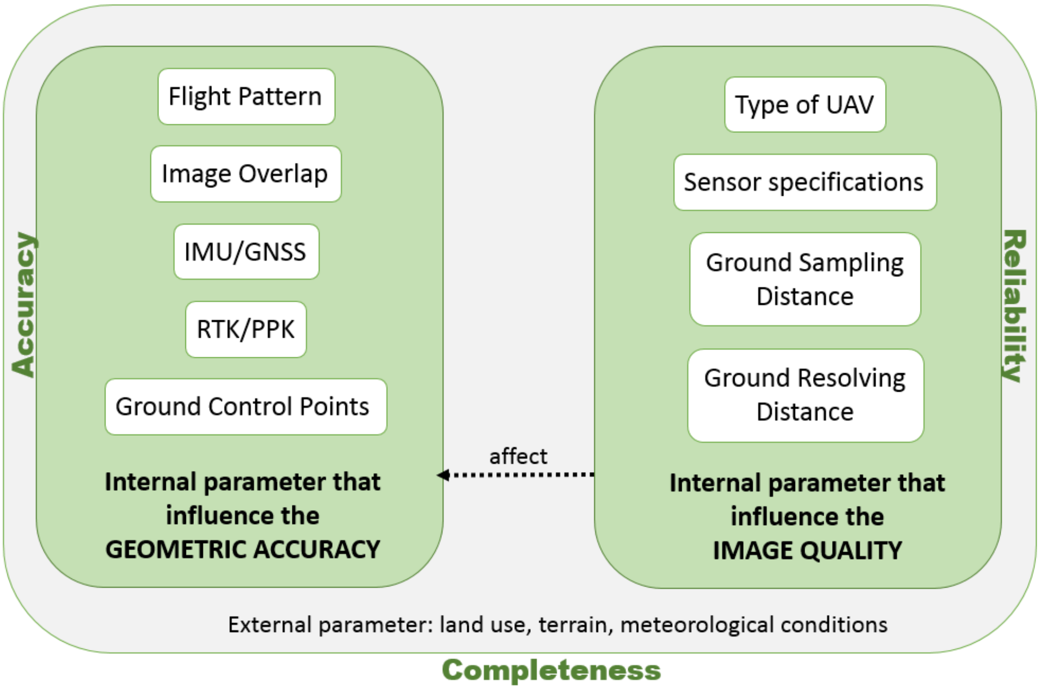

Figure 13: Schematic overview of quality metrics and influencing parameters

4.1 Reliability

As already outlined earlier - in the context of UAV-based orthomosaics - reliability can be interpreted as the representation of the real world. In this regard, the reliability is highly dependent on the image quality as the images provide the raw information for the photogrammetric pipeline which ultimately leads to the final orthomosaic. Thus, the following paragraphs discuss the properties of imaging sensors, flight systems, and resulting image qualities.

Sensor specifications

First of all, the physical characteristics of the imaging sensor determine the image conditions. Pixel pitch and focal length mainly influence the image resolution (i.e., ground sampling distance). The pixel pitch is the distance from the center of one pixel to the center of the next and can be calculated with the known sensor width and sensor resolution; i.e. the larger the pixel, the less exposure time it needs to receive all necessary light to capture the required information. Thus, a large pixel pitch has the advantage of comparatively short exposure time and thus potentially less motion blur. The comparison in Table 6 reveals the full spectrum of utilized sensors with different sensor sizes and pixel pitches. The example of the DT18 shows one negative trade-off: the large pixel pitch is borne by a low sensor resolution which leads to a smaller image footprint and involves more flight trajectories to achieve the required areal coverage.

Table 6: Sensor characteristics and luminosity histograms

	3DR Iris+	**DT18**	**Ebee PLUS**
Camera	Canon Power SX 260 HS	DT18 RGB	S.O.D.A
Sensor size	6.16 x 4.62 mm	8.45 x 7.07 mm	12.75 x 8.5 mm
Pixel pitch	1.54 µm	3.45 µm	2.33 µm
Sensor resolution	3000 x 4000 (12MP)	2448 x 2048 (5MP)	5472 x 3648 (20 MP)
Example image			
Lumi-nosity histogram of the grayscale example image	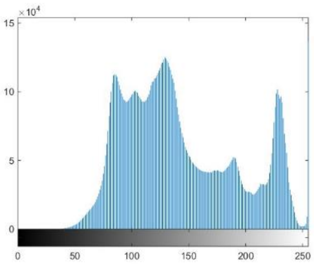	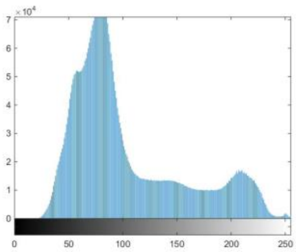	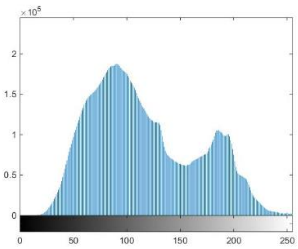
	GerMAP	**InspirePro**	**FireFLY 6**
Camera	Ricoh GR	DJI FC6520	SONY ILCE-6000
Sensor size	23.6 x 15.7 mm	13 x 17.3 mm	23.5 x 15.6 mm
Pixel pitch	4.79 µm	2.48 µm	3.92 µm
Sensor resolution	4928 x 3264 (16 MP)	5280 x 3956 (20.1MP)	6000 x 4000 (24 MP)

Example image			
Lumi-nosity histogram of the grayscale example image	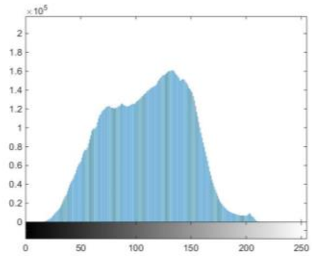	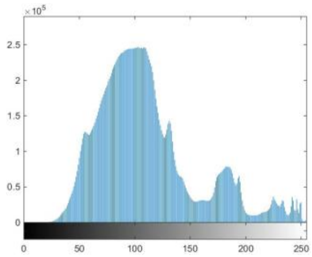	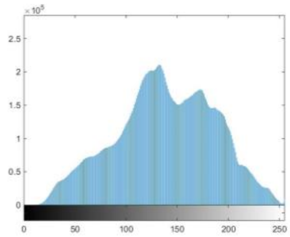

The histogram of the greyscale pixel intensity provides a quantitative measure to assess the luminosity of the image. Ideally, the histogram should be equally stretched across the dark and light tones (x-axes) without a peak close to 0 (underexposed) or close to 256 (overexposed). Since those pixels include hardly any texture which can be differentiated, the performance of the tie point extraction and image matching algorithm are negatively impacted. Challenging environments include corrugated iron roofs or water bodies which are highly reflective. This condition becomes visible in the small histogram peaks between luminosity values 200-256 of the image taken by the Inspire Pro.

Figure 14 provides some insights into the first processing results and compares the median number of extracted keypoints per image using different sensors. Here, the two sensors with the lowest resolution DT18 camera and 3DR Iris show also the lowest number of extracted tie points. This can be explained by the fact that images with a low sensor resolution show less feature and characteristics of the landscape to extract keypoints. Although FireFLY shows the highest sensor resolution (24MP), it shows on average less extracted keypoints than the Ebee Plus (20MP), GerMAP (16MP) and the Inspire Pro (20.1MP).

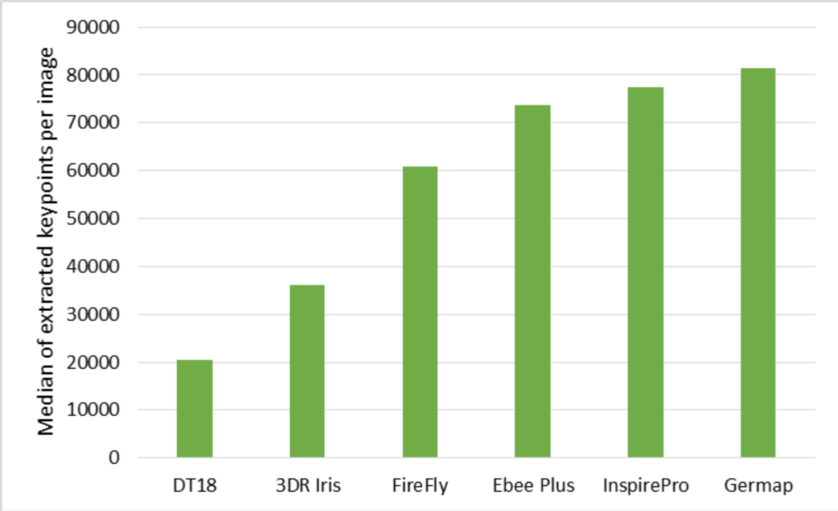

Figure 14: Comparison of extracted keypoints per image using different sensors

Type of UAV

An image represents an accumulation of light received by the camera sensor during a particular period. Ideally, the exposure time should be fast enough to capture a picture that appears as an instantaneous moment. However, this is not always the case and the movements of the camera during the exposure time result in a blurred image that provides less detail (Fig. 15).

Figure 15: Left: Image without motion blur; Right: Image with high motion blur

Motor vibration or the constant cruising speed during the flight can affect the sharpness and contrast of the images. During all UAV demonstration and data acquisition flights for the its4land project, one could observe three main modes:

- Rotary wing UAV with a stop and go flight mode: UAV flies to a waypoint and hovers to capture the image. Motion due to cruising speed is eliminated, but motor vibrations of (at least) four motors are still present.
- Fixed-wing UAV: flies with a constant cruising speed and captures images either during a specified time interval or when it passes predefined waypoints. DT18 and FireFLY follow this strategy.

- Sensefly: developed a particular wave-like flight path to tackle the challenge of motion blur. Before the UAV arrives at the waypoint, the Ebee ascends and stops the motor to capture the image. During this, it descends back to the predefined flight height.

Spatial resolution

The concept of the spatial resolution includes two different aspects: the ground sampling distance (GSD) and the ground resolving distance (GRD). The Ground Sampling Distance (GSD) is the distance between two consecutive pixel centers measured on the ground and is determined by the sensor specifications and the flying height. GRD is defined as the size of the smallest element distinguishable on an acquired image. The GSD value is only affected by the sensor's pixel size and the image scale, whereas GRD is not merely affected by these parameters but also by other aspects such as lens quality, lens aperture being used, and image blurriness. The GRD represents an essential metric for the sensor quality assessment as it demonstrates the level of information that can be derived from the image and subsequently the final orthomosaic. (Orych 2015) presents different methods to assess the GRD. His analysis has shown that the binary Siemens Star (Fig. 16) can be preferred when examining the capabilities of digital aerial sensors as it does not require laboratory settings and specific flight directions.

Figure 16: Siemens star and ground reference target

Due to its circular shape, the Siemens Star can be used to determine the resolution in all directions and in a fast and objective manner. While the outer edge shows the lowest frequency of the contrasting black and white pattern, the spatial frequency increases with the decrease of the radius. As the frequency increases, the image of this pattern will firstly become slightly defocused shown by a decrease in the amplitude of intensities of the black and white elements. By determining the star radius at which elements cannot be distinguished anymore (amplitude falls to zero), it is possible to calculate the ground resolving distance of the imaging sensor (Orych 2015). This test has been visually interpreted for four different flying heights using the Ebee Plus in Zanzibar. During all different flying heights, the wind and illumination conditions were similar. The Siemens Star was printed on a non-reflecting waterproof paper with a size of 1 m (Fig. 16).

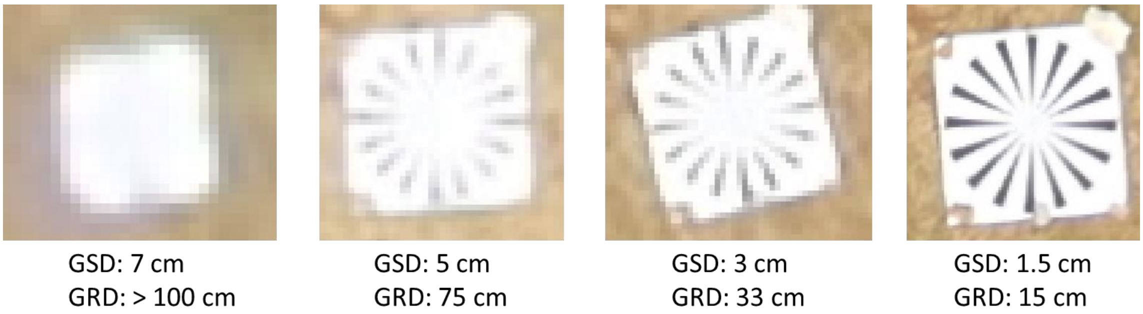

Figure 17: Comparison of GRD and GSD for different flight heights

For the test dataset, it can be shown, that the GRD is at least ten times the GSD. Interestingly, the ratio between GRD and GSD increases with the pixel size (cf. Fig 17). Although not tested during this field campaign, (Riza Nasrullah 2016) shows considerably smaller ratios for rotary wing UAVs. The discrepancy between GSD and GRD should be considered during flight planning.

As the Siemens Star was not always available to all datasets, the intensity profile along the black and white pattern of the deployed ground reference points was used to examine the differences between the sensors. Those specific ground markers were used during four out of six UAV field campaigns and were the only identical feature among the various UAV datasets. The position of the center point was manually extracted and respective profiles were automatically generated following the schematic sketch in Figure 18.

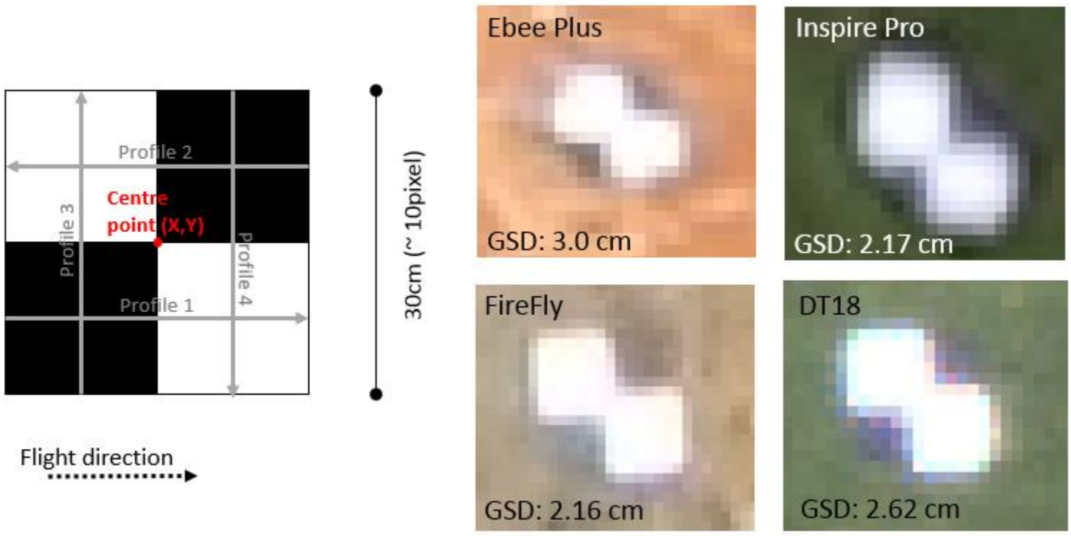

Figure 18: Strategy to extract intensity profiles of ground marker pattern on the left. Visual representation of ground marker in different datasets is shown on the right.

The visual representations in Figure 18 show already significant differences in the appearance of the ground marker. Although the GSD of the FireFLY and the InspirePro are similar, contrast and sharpness differ. DT18, as well as the FireFLY, clearly distinguish the black and white pattern whereas a somewhat continuous transition between black and white is observed with the InspirePro. Intensity histograms in Figure 19 quantify the spatial resolution. Here, the DT18 and FireFLY show steep curves between 8 to 10 pixels and need only two to three pixel for the transition between black and white. Although the InspirePro presents the highest contrast (highest range of greyscale values in all histograms), the edges are not clearly defined and the image appears blurred. All histograms except the histogram of the Ebee Plus do not show direction dependent sharpness differences. For the Ebee Plus, the lower right white quarter indicates less sharpness than the upper left. However, the rather low signal-to-noise ratio can partly be ascribed to the comparatively low resolution (3 cm).

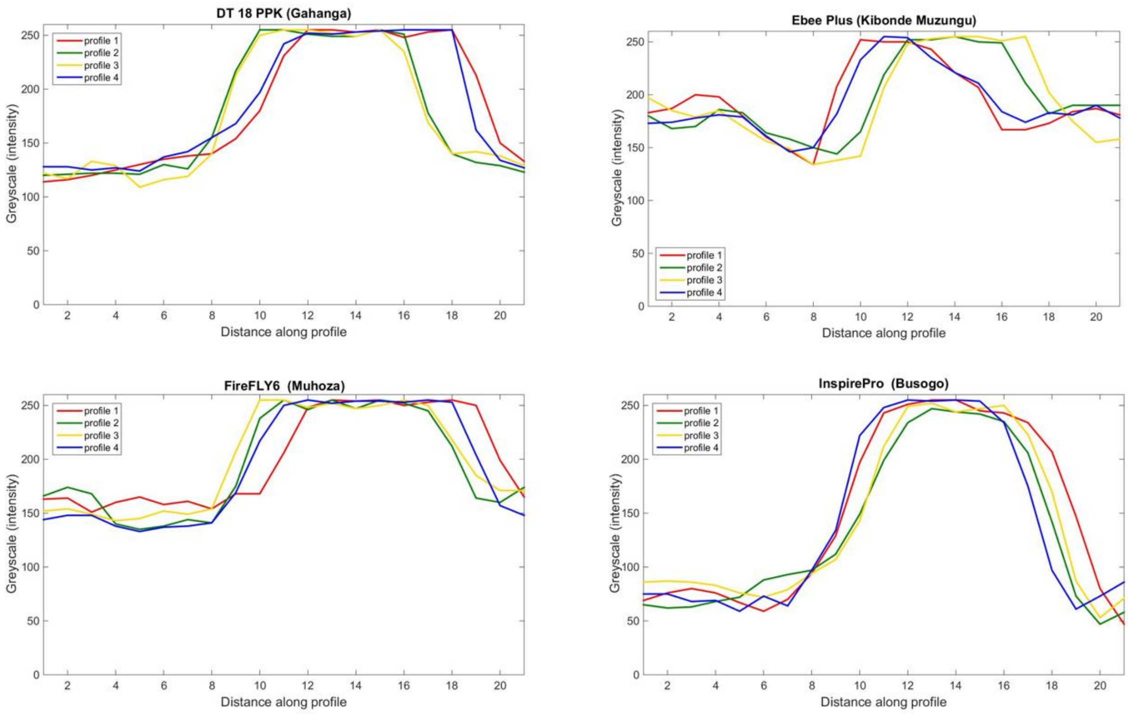

Figure 19: Intensity profiles of ground marker of four different datasets. Each color represents one particular direction as explained in Figure 18.

4.2 Accuracy

The parameters that affect the final geometric accuracy of the produced orthomosaics are described in two different ways. Firstly, one dedicated dataset of the DT18 obtained in Germany is used for a systematic evaluation of different processing scenarios. The second way includes an analysis that compares different sensors and different datasets against each other.

Comparison of different georeferencing strategies using one test dataset[1]

The UAV image dataset embraces eight different scenarios as shown in Table 7. Evidence about the final geometric accuracy and the overall performance is gained from several results: (1) checkpoint residuals, (2) comparison of EO parameters for the various scenarios, and (3) point cloud characteristics using a point-to-plane-based analysis (Fig.20).

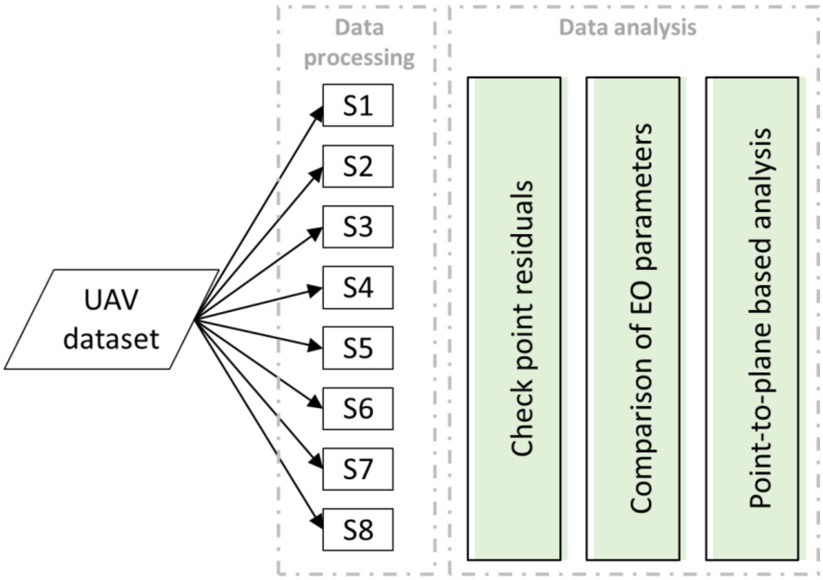

Figure 20: Schematic overview of the analysis

The first two scenarios (S1 and S2) encompass indirect georeferencing, i.e., without using the GNSS observations on board the UAV and thus follow the classic photogrammetric approach that uses automatic aerial triangulation (AAT) and bundle block adjustment (BBA) with ground control points to determine the EO parameters. S1 and S2 are distinguished by their number of GCPs. The subsequent four scenarios (S3-S6) are characterized by integrated data processing using GCPs as well as IMU/GNSS information. Here, raw data of the APX-15 system as well as PPK data were taken into consideration. Finally, the remaining two scenarios S7 and S8 follow the approach of direct georeferencing without using GCPs. To assess the quality of the calculated EO parameters, different weights were allocated. X, Y, and Z coordinates were assigned with high weights for S3 – S8 whereas high and low weights for orientation parameter alternated (cf. Table 7). Settings were adjusted in the image orientation options of Pix4D. As soon as GCPs were introduced (S3 – S6), the entire block geometry and thus also the

[1] This work has been presented at the UAVg conference in Bonn, 2017

EO parameters became optimized. The weight for enabled GCPs (S1 – S6) was set to 3cm in the horizontal and 5cm in vertical accuracy, respectively.

Table 7: Overview of processing scenarios

Scenario	EO data	EO parameters: assigned weight for image orientation		GCPs	CPs
		X,Y,Z	Ω,Φ,Κ		
S 1	none	-	-	18	4
S 2	none	-	-	4	18
S 3	raw	high	low	4	18
S 4	raw	high	high	4	18
S 5	PPK	high	low	4	18
S 6	PPK	high	high	4	18
S 7	PPK	high	low	0	22
S 8	PPK	high	high	0	22

With regard to the interior orientations parameters, these were delivered by the UAV manufacturer as approximations which were adjusted during the data processing using self-calibration.

Data analysis

Evidence about the final geometric accuracy and the overall performance was gained from different results obtained: (1) checkpoint residuals, (2) comparison of EO parameters for the various scenarios, and (3) point cloud characteristics using a point-to-plane-based analysis.

1) **Checkpoint residuals:** The conventional way to evaluate the geometric accuracy is the use of individual check points that were not taken into account during image processing. At this, the residuals are considered as the difference between the observed values and the model values. Here, check point coordinates serve as observed value and the calculated point position after photogrammetric processing as a value in the model. Mean and standard deviation of check point residuals provide findings of the geometric accuracy and allow to detect systematic shifts and block deformations. Conditioned by the definition of different scenarios, the number of considered checkpoints for this statistical evaluation varied.
2) **Comparison of EO parameters:** The second approach targets exploring the data processing performance of the various scenarios and encompass the comparison of EO parameters. Using this approach, one can determine positional uncertainties of projected points on the ground. The scenario with the lowest residuals at the check points will serve as a reference dataset. Differences of EO parameters were computed for the intersection of all images that were considered in all scenarios.
3) **Point-to-plane based analysis:** In addition to the conventional approach of using check points to assess the orientation quality dense image matching point clouds were compared. The approach follows the idea that if same dense matching

techniques are applied for each BBA-configuration (same imagery, same settings, but just different input IO/EO parameters), the differences in quality of the resulting point clouds is triggered in particular by the IO/EO parameters. This allows completing a relative accuracy check, even without reference points. To this end the method described by (Nex et al. 2015) was applied to perform a point-to-plane-based analysis, resulting in signed point distances to planes, where the point cloud from the best BBA-configuration was used as a reference. This enabled to determine the differences of systematic and random errors contained in the data.

EO parameters for S5, S6, S7, and S8 were post-processed using the software tool POSPac UAV from Applanix. During this step, the raw orientation values were corrected with RINEX data of a virtual GNSS reference station in the center of the study area. After running the calculations, POSPac provided performance metrics that included the RMSE of positional/angular differences for the post-processed EO parameters for each second of a flight. Statistics of this performance metrics are outlined in Table 8 and deliver evidence of a clear improvement: uncertainties of positional parameters of more than one meter in the raw dataset were minimized to a few centimetres in the PPK dataset. The same applies to angular values which were largely improved. Lowest accuracies were detected during flight turns where the IMU had difficulties to follow the change in direction which in succession led to higher uncertainties in the IMU/GNSS values than during smooth and straight sections of the flight lines. Especially banked turns can block the view of the satellites from the GNSS antenna. However, maximum RMSE values for all positional observations are still below 3cm. This performance can be ascribed to the high quality of the APX-15 IMU device and the embedded Inertially-Aided Kinematic Ambiguity Resolution (IAKAR) technology (Hutton et al. 2008; Scherzinger & Hutton n.d.).

Table 8: Performance metrics for real-time reference frame (raw) and post-processed smoothed-best estimated trajectory (PPK)

	Raw		PPK	
	Mean	Sigma	Mean	Sigma
RMSE north [m]	1.207	0.020	0.017	0.001
RMSE east [m]	1.213	0.022	0.011	0.001
RMSE height [m]	2.660	0.004	0.023	0.002
RMSE roll [arc min]	9.023	1.346	2.398	0.557
RMSE pitch [arc min]	8.855	1.118	2.606	0.583
RMSE yaw [arc min]	30.214	4.381	9.904	2.340

Evaluation of checkpoint residuals

As shown in Table 9 all scenarios are characterized by diverse statistics of the check point residuals.

Table 9: Mean and Sigma of checkpoint residuals separated by scenarios

		X	Y	Z
S1	Mean [m]	0.084	0.269	1.512
	Sigma [m]	0.187	0.429	3.040
S2	Mean [m]	-0.242	-0.055	-9.284
	Sigma [m]	1.646	1.062	10.757
S3	Mean [m]	0.124	0.042	0.107
	Sigma [m]	0.122	0.156	0.362
S4	Mean [m]	-0.075	1.072	0.696
	Sigma [m]	1.113	0.816	0.560
S5	Mean [m]	0.001	0.008	0.033
	Sigma [m]	0.032	0.024	0.152
S6	Mean [m]	-0.757	0.571	0.492
	Sigma [m]	1.159	0.948	0.549
S7	Mean [m]	0.217	0.186	0.053
	Sigma [m]	0.034	0.028	0.148
S8	Mean [m]	0.156	0.502	0.727
	Sigma [m]	1.225	0.955	0.244

Surprisingly, the conventional photogrammetric method with AAT and BBA in S1 does not deliver the expected geometric accuracy. Although 18 equally distributed GCPs were considered for the image processing, check point residuals for this scenario are characterized by a comparatively high standard deviation. In contrast to the remaining scenarios, S1 and S2 – those scenarios without initial EO parameters – present a significant difference of the horizontal and vertical accuracy values. This verifies the assumption that initial EO parameter approximations support tie-point extraction, accurate height reconstruction and finally avoid large block deformations.

The remaining six scenarios display a systematic pattern, and one can clearly distinguish those scenarios with a high weight on angular values and those with a lower weight. When positional, as well as angular EO parameters, are considered with a high weight (S4, S6 and S8), significantly fewer tie-points can be found among matched images. For all these three scenarios, the values for the standard deviation of the horizontal position is in the range of 1m. High mean values also give evidence to high block deformations. A close look at S4 and S6 embraces that both horizontal accuracies are at the same range even though S4 was calculated with raw EO parameters and S6 with more accurate PPK data. These results show that the high weight of the angular values affects the tie-point extraction and the image orientation negatively as it constrains the search for homologous points and furthermore the convergence towards minimized reprojection errors during the BBA.

The results of S3, S5, and S7 – those scenarios where only positional EO parameters were assigned with a high weight and angular values with low weight – reveal higher geometric accuracies that go down to pixel level (GSD 2.8cm). In contrast to the statistical distribution of S4, S6, and S8, the PPK option shows substantial improvements of the block stability proven by low sigma values of S5 and S7. In addition, the height component could be reconstructed more reliably with the PPK corrections. High mean and low sigma values for S7 indicate a systematic shift that can be explained by the absence of GCPs. S5 stands out for the lowest mean and sigma values and thus represents the scenario with the highest geometric accuracies and is therefore chosen as the reference dataset (see 4.3 and 4.4.).

Comparison of EO parameters

For this analysis, differences to the reference dataset S5 were computed per image for all six EO parameters. Statistics of this relative quality measure are summarized in Table 10 and provide the first overview before the parameters are analysed in more detail.

Table 10: Mean and RMSE of EO parameter differences

		x [m]	y [m]	z [m]	Ω [°]	Φ [°]	K [°]
S1	Mean	0.021	0.222	-1.060	-0.135	0.021	0.003
	RMSE	2.735	2.029	4.765	1.263	1.665	0.167
S2	Mean	0.078	-2.601	2.899	1.626	-0.475	0.214
	RMSE	5.197	4.228	21.063	2.851	4.086	0.462
S3	Mean	-0.169	0.147	2.836	-0.089	-0.005	-0.003
	RMSE	0.352	0.434	2.875	0.247	0.170	0.075
S4	Mean	-0.071	-0.503	0.110	-0.175	-0.166	0.061
	RMSE	0.308	0.727	0.776	0.271	0.665	0.270
S5	reference dataset						
S6	Mean	0.551	-0.285	0.108	-0.048	-0.074	0.041
	RMSE	0.627	0.422	0.383	0.194	0.663	0.102
S7	Mean	-0.208	-0.171	-0.053	-0.004	0.006	-0.001
	RMSE	0.208	0.172	0.068	0.006	0.008	0.008
S8	Mean	-0.208	-0.171	-0.053	-0.095	-0.024	0.040
	RMSE	0.208	0.172	0.068	0.211	0.660	0.102

In comparing the results of the check point residuals, S1 and S2 stand out for their high RMSE values which are up to one decimal power higher than for the remaining scenarios. Compared to the PPK options, the raw data option of S3 and S4 shows higher RMSE values at the z-component which mirror the high uncertainties of the raw GNSS observations. Since no GCPs were introduced for S7 and S8, positional parameters (x, y, z) were not optimized during BBA and remain the same for both scenarios. S7 exhibits the lowest differences to the reference dataset.

As the EO parameters are not independent of the IO parameters, Table 11 displays the focal length that was calculated during self-calibration. Furthermore, the mean reprojection error provides a suitable measure to indicate the quality of the tie-points matching and the “tension” with external constraints (GCPs, GNSS, and IMU information). In this regard, the high weight set for the orientation parameters in S4, S6, and S8 does constrain the BBA and the self-calibration of the camera providing different focal lengths and higher re-projection errors.

Table 11: Focal length (f) and mean reprojection error (R) of BBA

	S1	S2	S3	S4	S5	S6	S7	S8
f [mm]	12.09	12.11	12.40	12.0	12.03	12.0	12.03	12.0
R [pixel]	0.134	0.134	0.268	0.561	0.102	0.506	0.102	0.506

The following two figures (21 and 22) reveal a detailed investigation of the variabilities of the EO parameters during the entire image acquisition flight. Since the angular values are in the main interest of this paper, only *Omega* and *Phi* were selected for a graphical representation. As evident from Table 9, S1 and S2 are in a different range and were not considered for the following comparison.

Differences in *Omega* and *Phi* – as visualized in Figures 21 and 22 – show a similar systematic pattern for S4, S6, and S8 as the angular values provided by the IMU have a substantial weight in the BBA and their values are almost the same. Positive and negative peaks for those scenarios change at each flight turn of the UAV and stay during straight lines with a constant offset of +0.1/ -0.2° for *Omega* and +/- 0.7° for *Phi*. The systematism could be attributed to a small misalignment between the sensors which can be corrected when the angle parameters have less weight during the image orientation process. In contrast, differences for S3 do not show such a systematic pattern which can easily be correlated to the flight strips. For the *Phi* observations, the minimum and the maximum peaks for S3 remain lower than the peaks of S4, S6, and S8, respectively. In this case, the differences are mainly due to compensating the different information provided by the raw GNSS data. As expected from the RMSE values, S7 displays almost identical angular orientation parameters.

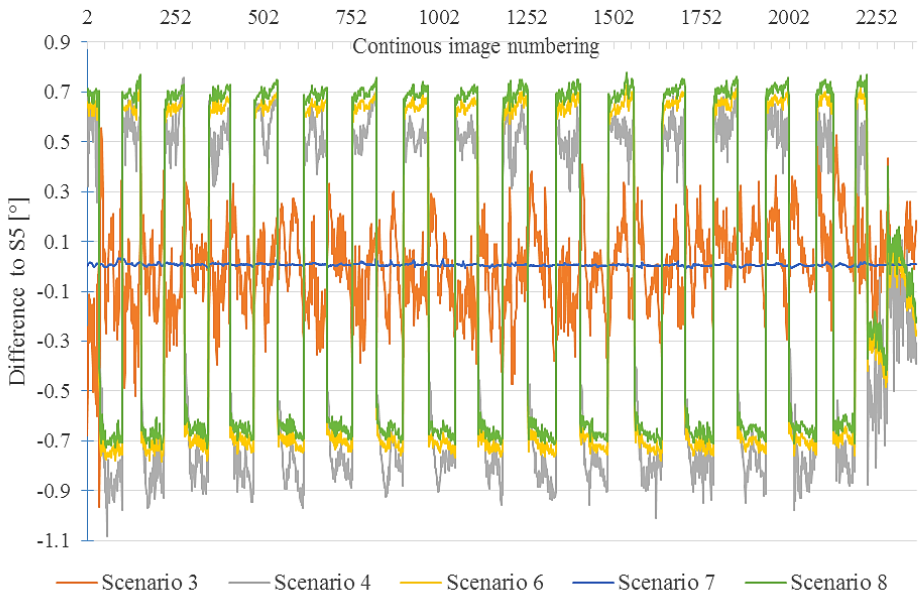

Figure 21: Differences in Omega

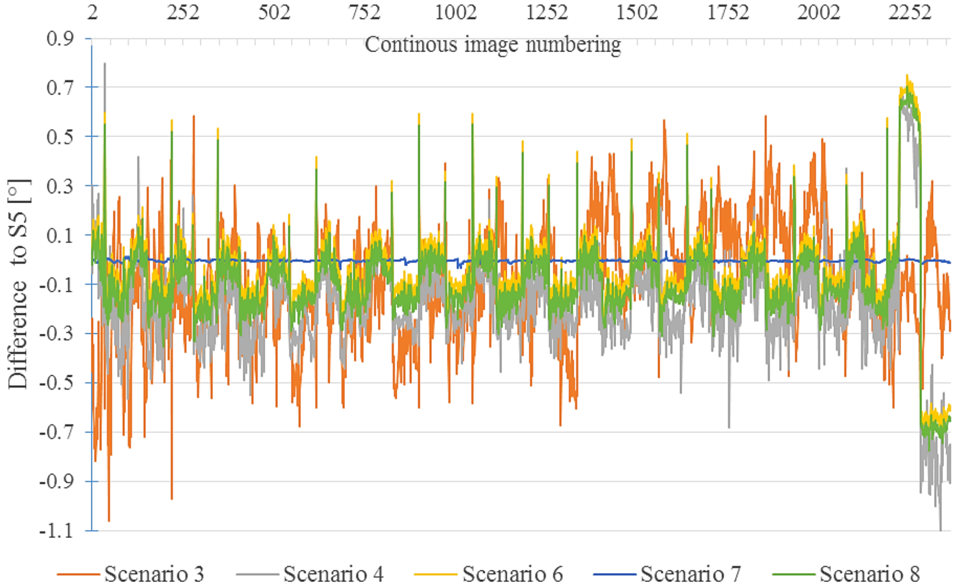

Figure 22: Differences in Phi.

Point-to-plane analysis

As described earlier, this analysis focuses on the comparison of extracted planes. Since land covers such as meadows, forests and fields are too noisy for the required planarity of this analysis, dedicated subareas with planar features such as roofs, paved roads, and walkways were extracted. These areas include a farm, the monastery 'Benediktinerabtei Gerleve' and the building of the restaurant (Fig. 23).

Figure 23: Selected areas for point-to-plane based comparison

Depending on the performance of the BBA the quality of dense matching outputs varied. Thus, not all selected planes showed sufficient point densities to be suitable for the point-to-plane analysis. Due to its high vertical offset S2 was not considered in this comparison since respective planes could not be assigned to each other. The number of matching planes is shown in Table 12 and reveals insights into the data quality of reconstructed point clouds. S4, S6, and S8 show the smallest number of matching planes. This result can be ascribed to the fact that predefined angular EO parameters are still too erroneous and limit the detection of homologous points during the image orientation process. As an example, only half of all selected reference planes could be matched for S4.

Table 12: Number of matching planes that were included in the point-to-plane analysis

	S1	S3	S4	S6	S7	S8
Number of matching planes	90	105	63	77	92	80

As a recurrent phenomenon in the results, extracted planes of S4, S6 and S8 show a high mean standard deviation for the point-to-plane distances (see Fig.24). This indicates a high level of noise and can be attributed to the poor quality of the input point clouds. In contrast, the results for S1 display a high systematic error (higher mean orthogonal distance than the mean standard deviation) that can be ascribed to the high positional offset. S3 shows the only positive value for the mean orthogonal distance and indicates a systematic shift. This can be explained by the fact that the EO parameters were based on raw observations that entail markedly higher positional uncertainties. S7 proves to be the scenario with the lowest positional offset although the value of the mean standard deviation indicates noise.

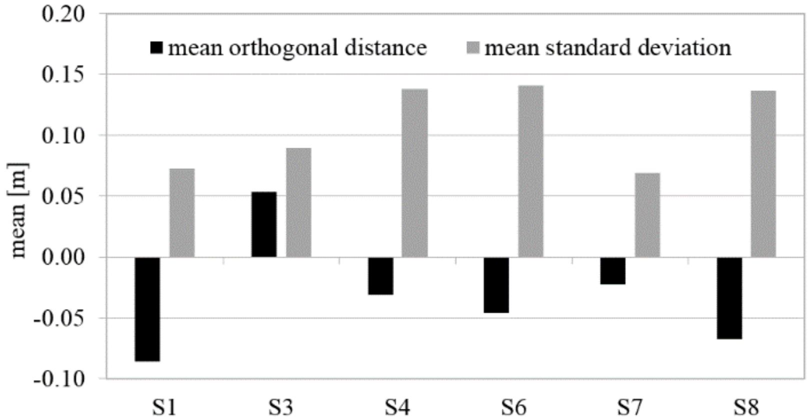

Figure 24: Statistics of signed point-to-plane distances separated by scenarios

All results show clear evidence that known EO parameters (delivered by the onboard sensors) are beneficial to guide the tie-points matching, especially when the obtained UAV images impose challenges to the conventional AAT approach. This includes poorly textured areas, changing illumination conditions during the flight, and motion blur or image noise. Even with a dense network of GCPs, it was not possible to obtain the same level of accuracy as with the use of raw EO parameter approximations. The use of the post-processed APX-15 GNSS and IMU data was particularly beneficial to enhance the data quality at pixel-level of the horizontal accuracy. However, it was also shown, that the angular EO parameters are still too inaccurate to be assigned with a high weight during the image orientation process. Furthermore, detailed investigations of the EO parameters during the entire image acquisition flight unveil systematic sensor misalignments and offsets. This type of errors could easily be fixed with a dedicated calibration of the lever arm of the system. With highly accurate IMU/GNSS observations, the need of ground truthing can be reduced to a minimum of only 4 GCPs which are needed to avoid a systematic positional (mainly horizontal) offset of the dataset. Time-consuming field work to measure high quantities of GCPs becomes obsolete and makes large-scale UAV mapping a more feasible solution for practitioners that require high geometric accuracies.

Comparison of influencing parameters on final accuracy using multiple UAV datasets

Image overlap

In most cases, the image block is composed of different strips, and one distinguishes the forward (or along-track) overlap and the side (or across-track) lap. The forward overlap defines the overlap between images on the same flight strip, while the side lap determines the overlaps between images belonging to adjacent strips. Image overlap is specified during the flight planning and impacts the number of images, duration of the flight and the block stability of the images during photogrammetric processing. The minimum mathematical overlap among adjacent images should be at least 50%, to ensure that one object is at least visible in two images. Whereas the forward overlap can be increased without additional flight strips, the side lap determines the length of the flight trajectory and how many flight strips are needed to capture the area of interest. However, a large forward overlap will lead to another additional issue; it creates more images for the same sized area. Ultimately, this vast number of images will lead to other extra costs: processing time and processing tools. Thus, the definition of the required overlap should be assessed according to the goal of the flight and the user needs. Commonly recommended setups are 70% forward overlap and 60-80% side lap (Colomina & Molina 2014).

During the test flights in Zanzibar, three different side lap were selected, 60%, 70%, and 80%, in order to demonstrate their impact on the photogrammetric processing. Figure 25 shows one main consequence – a high overlap increases the overall number of tie points of the image block. For 80% side lap, 2236145 tie points were extracted compared to only 1637922 for the 70% side lap and 1219724 tie point for the 60%. A high number of tie points between images provides a better stability in the bundle block adjustment and reduce mismatches. Furthermore, a single position on the ground will be mapped in more images than with a smaller overlap, helping to reduce 3D positional ambiguity. Especially the multiplicity of tie points which are visible in more than two images will eventually increase the rigidity of the block and are preferable to simple tie-points.

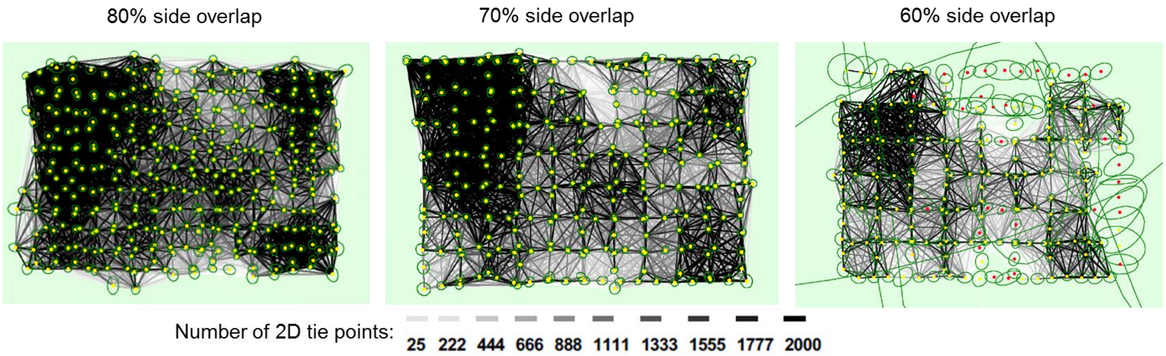

Figure 25: Visual representation of tie points between images (yellow dots) for three different side laps. Bright links indicate a low number of tie points and dark links indicate a high number of tie points.

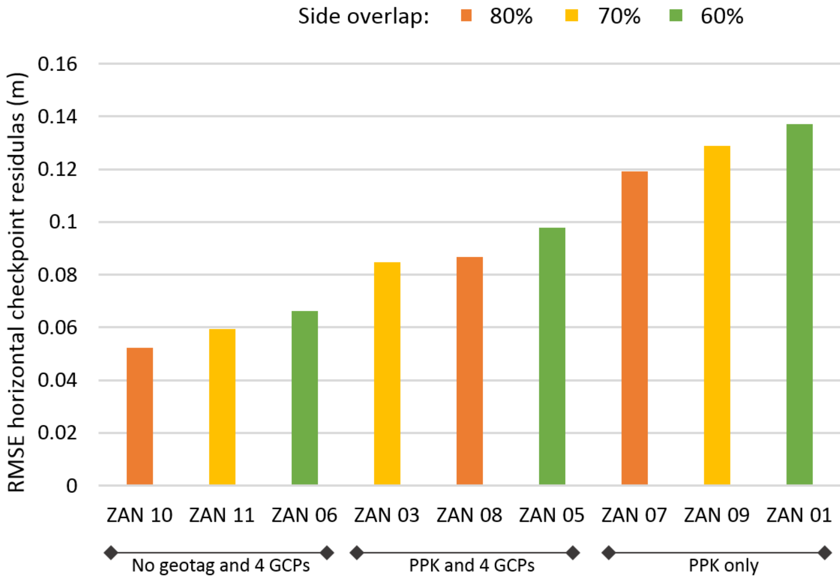

Figure 26: Influence of different side laps on the geometric accuracy

Figure 26 shows the impact on the final geometric accuracy derived from independent check points. While the 80% side lap increases the final accuracy for the processing scenarios without geotags and with only 4 GCPs, as well as for the PPK geotag information without GCPs, it does not increase the accuracy for the scenario with the PPK and additional GCPs. This can be explained by the fact, that PPK geotags and additional GCPs already increase the image block robustness and compensate for the lower number of tie points with 70% side lap. In all three cases, 60% side lap shows the lowest accuracy.

IMU/GNSS and PPK/RTK option

The advantages of PPK to the final accuracy are already comprehensively outlined in section 3.2.1 including a detailed analysis of one dataset of imagery captured with the DT18 in Germany. However – since not all users can afford a high-quality IMU/GNSS which is capable of RTK or PPK workflows – the following comparison will evaluate the performance of the geotag information which is extracted from the on-board GNSS of different UAV platforms. All datasets in this comparison have a side lap of 70 %. The georeferencing of the image block is solely based on the logged GNSS coordinates during the flight.

The bar diagram in Figure 27 shows high discrepancies in the achieved horizontal accuracy. The datasets of the Ebee Plus and DT18 reach a final RMSE of less than 1m without PPK/RTK and even below 30cm with PPK corrections of a local GPS base station. Interestingly, the accuracy does not differ significantly among different spatial resolutions (3cm – ZAN09, 5cm – ZAN15, and 7cm – ZAN12). The UAVs used to date in the its4land project had different navigation and positioning devices. These are:

- ➔ APX-15 has a multi-frequency GNSS receiver
- ➔ EbeePlus operates with a dual frequency GNSS receiver

➔ InspirePro, 3DR Iris+ and FireFLY6 are equipped with a single frequency GNSS receiver

In contrast, the geotags of the 3DR Iris and the FireFLY only allow a final accuracy of more than 2m. Both datasets show a high potential to increase the accuracy with additional GCPs.

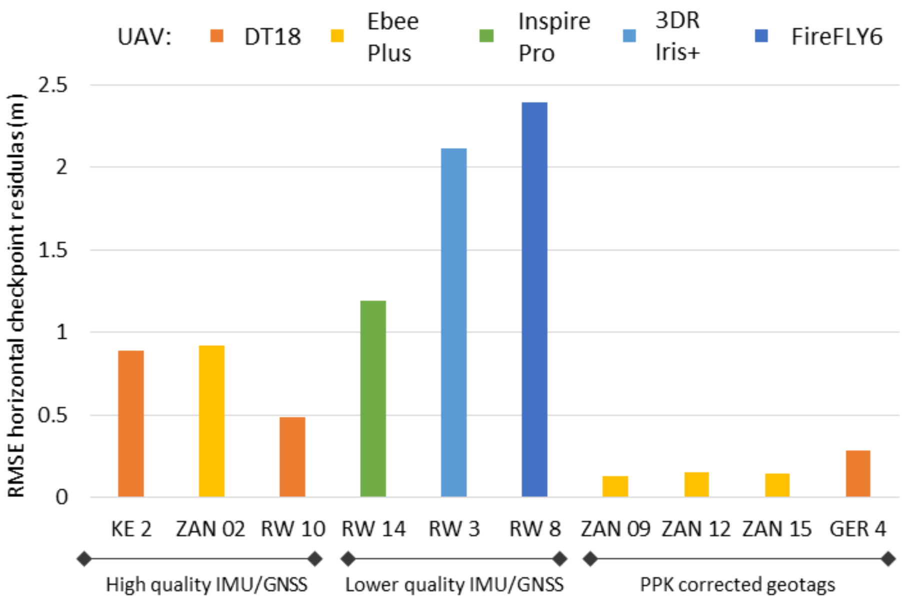

Figure 27: Influence of different geotag information on the geometric accuracy

GCPs

The influence of GCPs on the final accuracy of 3D point clouds, digital elevation models, and orthomosaics has been well researched over the past years (e.g., Tonkin & Midgley 2016; Agüera-Vega et al. 2017; Jóźków & Toth 2014). As for the image overlap, one can see a discrepancy between the theoretical minimum number of GCPs and the practical recommendations. Whereas three GCPs are the mathematical minimum to georeference the data products, as many as eight to twelve GCPs are recommended to achieve geometrically accurate results. Furthermore, this redundancy ensures good results also in cases where locals remove intentionally or nonintentionally some GCPs. All GCPs should be well distributed throughout the AOI (block) and not be clustered together. Following this, they should be in the center as well as near the edges, but not on the edges of the AOI as the image overlap decreases towards the edges. The test datasets for the evaluation of the impact of different GCP configurations on the final geometric accuracy meet the following criteria: 70% side lap, 70-80% forward overlap, flight trajectory without cross-flights and geotags without PPK corrections. Datasets were processed without GCPs, with 4 GCPs at the corner points and with 9 evenly distributed GCPs.

As already shown in the previous paragraph on the IMU/GNSS, the quality of the IMU and GNSS receiver has a significant impact on the geometric accuracy if no GCPs are involved in the georeferencing (i.e. zero number of GCPs). Four additional GCPs already correct systematic errors of the GNSS observations and can reduce the final RMSE of check point residuals (e.g., Ebee Plus), see Figure 28. For the FireFLY, InspirePro, and DT18 more than four GCPs result in an increase of the geometric accuracy. However, if the block stability and image quality are comparatively weak (e.g., 3DR Iris+), four or even nine GCPs do not solve the poor block robustness.

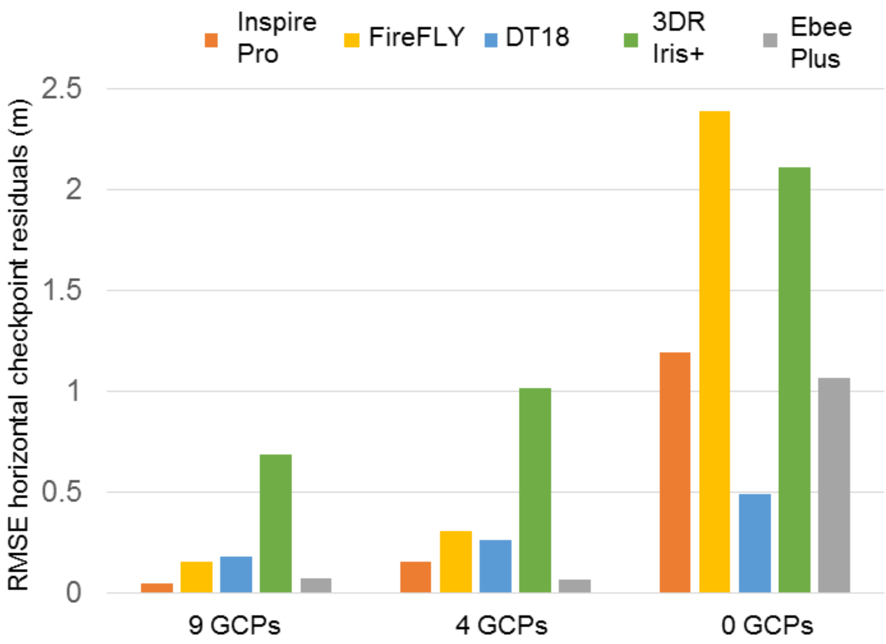

Figure 28: Influence of the amount of GCPs on the geometric accuracy

4.3 Completeness

The quality metric completeness includes both aspects – the completeness of one image block but also the completeness of a dataset captured during multiple flights. Both issues can be prevented by applying a large overlap – between corresponding images and between individual image blocks. However, land cover and specific wind conditions can demand even larger overlaps to ensure the completeness of the dataset.

Land cover

Land cover can strongly influence the photogrammetric reconstruction of a scene, particularly the extraction of tie points which are defined as homologous points between two or more images. Land cover with little texture such as sand, snow and forest entail challenges to image matching. Figure 29 exemplifies the small number of automatic tie points that were found in forested areas.

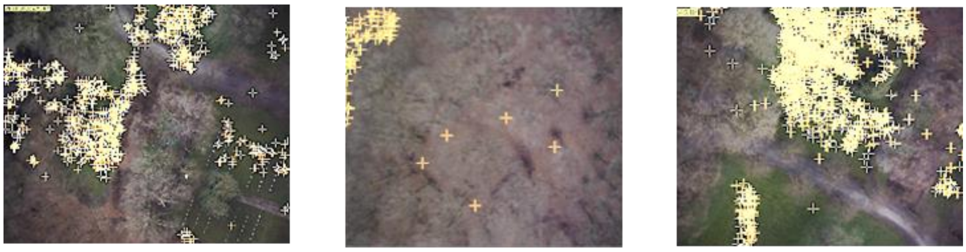

Figure 29: Examples for automatic tie points (crosses) on forest areas

A detailed investigation of the check points in Figure 30 shows that the lowest residuals are found in open areas such as agricultural fields, buildings or infrastructure. High residuals can be found in the vicinity to trees or at the margins of the study area. Here, ambiguous textures lead to poor results of the tie point extraction which in turn reduces the block robustness in these areas.

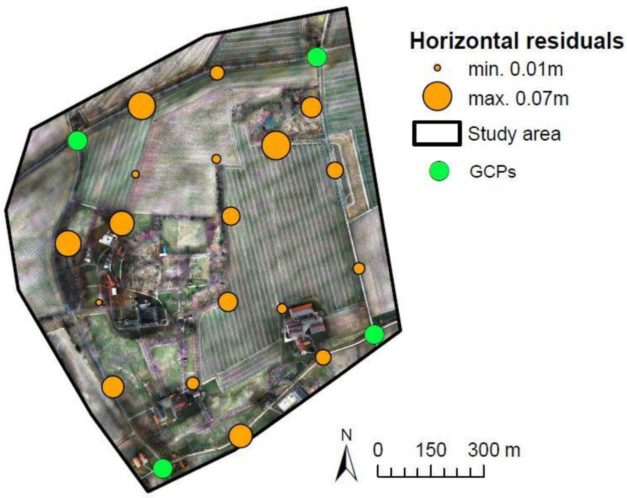

Figure 30: Horizontal residuals at check points (GER3)

Additionally to the tie point extraction, significant challenges can occur in urban areas or areas with high features (trees, high rise buildings) as they lead to occlusions on the ground. In this case, 80-90% forward overlap and at least 60% side laps are recommended to ensure a full stereoscopic coverage of the area.

Wind

Wind speed can profoundly influence the completeness of a UAV dataset. The first aspect relates to the flight performance of the UAV. Turbulences lead to adaptive flight maneuvers and waypoints might not be reached. Constant wind increases the power consumption of the engine and can reduce the flight time enormously. Side wind affects the orientation of the UAV as fixed wing platforms tend to correct their position against the wind. Slanted image footprints are the consequence with a reduced side lap. Especially for fixed wing platforms where the camera is triggered at a specified time interval, tailwind will lead to a reduction while headwind leads to an increase of the forward overlap. The effect on the position of the camera projection centers is illustrated in Figure 31 (middle). This example is taken from the DT18 flight in Kenya; with a cruising speed of 17m/s, a wind speed of 6 m/s resulted in a ground speed of 23m/s with tailwind and 11m/s with headwind. As a general indication, 8-10 m/s should be considered the maximum wind speed allowed to fly a UAV.

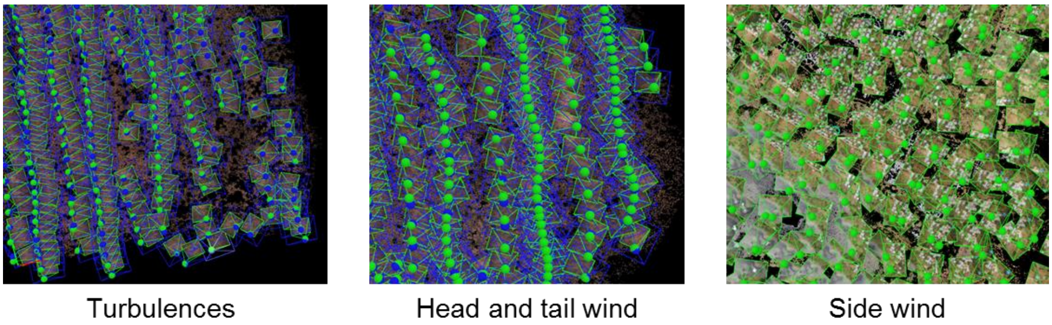

Figure 31: Effect of different wind conditions on the position of camera projection centers

A second aspect refers to the problem of moving features on the images. Especially trees are prone to move during wind which leads to severe problems during the image matching as no corresponding points can be found.

5. Manual on key flight scenarios

Based on the experience of the first its4land UAV flights in East Africa and the results of the systematic analysis of influencing parameters, one can distinguish four different flight scenarios for land tenure recording. As depicted in Figure 32, the scenarios are classified according to their characteristics with regard to spatial coverage and geometric accuracy. Exemplified use cases and UAV flight recommendations are outlined in the following subsections.

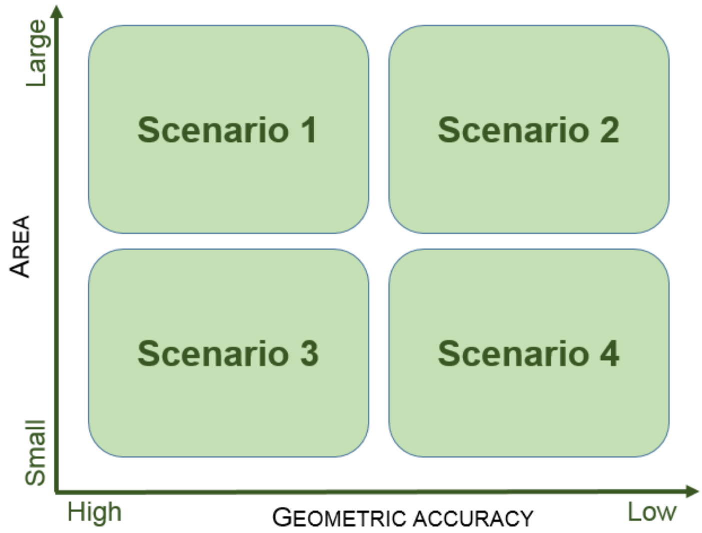

Figure 32: Schematic overview of defined key flight scenarios for land tenure recording

5.1 Scenario 1: large area and high geometric accuracy

One possible use case for this scenario refers to the revision of the National Development Plans (i.e., Master Plans) for Secondary Cities in Rwanda. National authorities expressed the urgent need for up-to-date aerial images to compare the planned developments with the current situation on the ground. Here, UAV imagery can be used to update the current base data which was mapped from aerial images acquired in 2009. The current base data is still being used as a decision-support tool although most of the data – especially in the urban areas – is already outdated. Demands on the accuracy are high as the UAV base data can be used to provide a spatial reference framework.

UAV flight recommendations – best practice

The vast extent of urban settlements necessitates the use of a fixed-wing UAV. If open flat spaces for landing the UAV are rare, the choice should be in favor of a vertical take-off and landing UAV, i.e. a hybrid UAV as this one can land on small open patches of a few meters. As the deployment and measurement of GCPs are very time-consuming for large areas and the risk of control points being removed is very high, the UAV should be RTK or PPK capable. If no national continuously operating reference network for GNSS corrections is available, a separate GPS base station should be used. Additionally, a minimum amount of ground reference points should be measured to assess the final accuracy or to correct systematic offsets in the IMU/GNSS observations. The camera of the UAV should ideally have a large sized sensor with a high resolution which results in a larger image footprint on the ground and ultimately fewer flight strips (ie less time needed to acquire the imagery). Image overlaps should be at least 70% to compensate for occlusions at high ground features and to achieve a rigid block geometry with a high number of corresponding points.

5.2 Scenario 2: large area and low geometric accuracy

This scenario depicts a use case from customary land tenure in Kenya. Group ranches are the present form of tenure and are only scarcely recorded. Here, UAV data can be used as a base map to sketch qualitative land and use rights (as performed under WP3) in the rural environment of Mailua (Kajiado). The land of a group ranch has an extent of several km². The terrain is moderately undulated with height differences up to 300m. Little thorny vegetation and bushes characterize the semi-arid landscape. The pastoralists live in round-shaped huts called “boma”. The boundary of the group ranch is usually demarcated using a continuous arrangement of thorn bushes.

UAV flight recommendations – best practice

Similar as for Scenario 1, a fixed-wing UAV is the choice to capture images of a large area of interest. Realistic flight times up to one hour allow mapping of several km² during one flight. As the requirement for high absolute accuracy is small, geotag information of a sophisticated IMU with dual frequency GNSS is sufficient. PPK and RTK are not considered as mandatory. Due to the slightly undulated terrain and rough meteorological conditions with constant wind and turbulence due to the landscape, one recommends image overlaps of 70%. Next to this, the flight plan should contain predefined waypoints instead of a constant time interval that triggers the camera as the waypoint-mode is less affected by windy conditions. Furthermore, the UAV should be equipped with a medium- to high-quality sensor as recurring features at the relatively texture-less landscape can course mismatches if the image quality is poor. Regarding effectiveness, the flying height should be chosen to achieve a GSD of a decimeter if the regulations allow the flight in this height.

5.3 Scenario 3: small area and high geometric accuracy

This scenario aims for high geometric accuracy while the expected spatial coverage for one flight mission is quite small. A possible use case includes an urban area with a high magnitude of land transactions and subdivisions. Instead of surveying all plots with the conventional ground surveying equipment, UAV imagery can provide a profound base map to manually or automatically define the updated spatial extent of a land parcel. A couple of UAV flights can be sufficient to cover the area at a high resolution.

UAV flight recommendations – best practice

As the spatial coverage does not determine the type of UAV, the UAV should be chosen according to the sensor specifications and the external conditions such as the meteorological conditions and available landing sites. However, the UAV should be capable of improving the geotags with GNSS reference data from a GPS base station. Since the area is comparatively small, RTK should work well as long as no high obstacles impede the transmission of the correction data via the radio link. The sensor is qualified through a high resolution (at least 16MP) to ensure that the boundary features such as particular plants, walls, hedges or fences are identifiable. Motion blur can be reduced while choosing a large pixel pitch which requires less exposure time to receive the same information since a small pixel pitch will require a long exposure time. Similar to scenario one, image overlap is a crucial aspect regarding the geometric accuracy. Large overlaps in both directions – forward and side – are recommended to be 80% to ensure a rigid image block.

5.4 Scenario 4: small area and low geometric accuracy

For this scenario, a hypothetical use case as discussed with several stakeholders in Rwanda and Kenya is suggested. Here, UAV-based information facilitates the constant monitoring of areas with high dynamics in urban developments. Frequent UAV flights can help to track the progress and to ensure that ongoing developments are in accordance with the plan.

UAV flight recommendations – best practice:

The recommendations for this scenario are comparatively straightforward. Any UAV with a GNSS and a camera on board is sufficient for this task. At any rate, images should be taken in the automatic flight mode with predefined trajectories according to the side lap. If the UAV is steered manually, the image overlap can vary enormously. Thus, the dataset might not be complete. Large block deformations or an incorrect reconstructed scene are the results. Since geo-localization is of minor importance, sole use of geotagging information can serve this purpose sufficiently. However, permanent ground markers can be established to assess the accuracy and to involve geo-locations of the GCPs into the photogrammetric processing, if needed.

6. Conclusion

Based on a literature review, three main quality metrics – namely accuracy, reliability and completeness – were extracted to assess the fitness-of-use and data quality of UAV-based products for land tenure recording. More than 40 datasets from 8 UAV field campaigns and demonstrations were used to correlate the final quality of the data products with the quality metrics.

Reliability is mostly affected by the image quality. Poor image quality results in weak performance of the photogrammetric processing and finally, the data product does not represent the real word as image block deformations, and erroneous surface reconstructions are inherent. Image quality is mainly determined by the sensor characteristics. However, also flying mode and spatial resolution impact the quality and quantity of information that can be extracted from UAV images.

Accuracy refers to a crucial metric when it comes to the assessment of data products for land tenure recording. Many jurisdictions impose a threshold for the maximum tolerable geometric accuracy of surveyed parcel boundaries. Depending on the required accuracy and the equipment at hand, this investigation outlines various strategies that can be followed to achieve the desired product quality. The scientific analysis included image overlap as well as different ground truthing strategies. We observed different final accuracies depending on the quality of the IMU/GNSS system. It was found, that the use of high-quality units with RTK or PPK capabilities can reduce the number of GCPs tremendously. Known locations of the camera projection centers are highly beneficial to guide the image matching even if the image quality is low. In turn, a reasonable number of GCPs can compensate the poor performance of the onboard system.

Completeness is mainly affected by external parameters such as land cover, terrain, and wind. Although the flight plan considers sufficient overlap, wind can impact the flight performance leading to gaps and insufficient overlap. Certain land uses such as forests, snow, and bare soils or feature such as corrugated iron roofs impose challenges to find corresponding tie points which lead to unsatisfactory results during the image matching. In both cases, a high image overlap and cross flights can prevent imperfection of the final results.

The manual on key scenarios assigns four specific scenarios according to spatial scale and geometric accuracy. User requirements are set by possible use cases in the its4land target countries. Insights of product specifications (i.e., orthomosaics) are gained from the analysis of influencing internal and external parameters. The four different scenarios are defined in such a way that the specifications meet the user requirements which – by definition (ISO 2013) – ultimately implicates a sound data quality.

Finally, the technical report on influencing parameters as well as the manual on key flight scenarios can be seen as a "code of conduct" for all future field campaigns that utilize UAVs for land tenure recording.

The following papers were published within the scope of this Deliverable:

1. Stöcker, C., Nex, F., Koeva, M., & Gerke, M. (2017). Quality assessment of combined IMU/GNSS data for direct georeferencing in the context of UAV-based mapping. *The International Archives of Photogrammetry, Remote Sensing and Spatial Information Sciences*, *42*, 355.
2. Stöcker, C., Ho, S., Koeva, M. N., Nkerabigwi, P., Schmidt, C., Zevenbergen, J. A., & Bennett, R. M. (2018). Towards UAV-based Land Tenure Data Acquisition in Rwanda: Needs Assessment and Technology Response. In *FIG Congress 2018: Embracing our smart world where the continents connect: enhancing the geospatial maturity of societies, Istanbul, Turkey, May 6-11, 2018* (pp. 1-17). [9428] Copenhagen: International Federation of Surveyors (FIG)

Bibliography

Agüera-Vega, F., Carvajal-Ramírez, F. & Martínez-Carricondo, P., 2016. Accuracy of Digital Surface Models and Orthophotos Derived from Unmanned Aerial Vehicle Photogrammetry. *Journal of Surveying Engineering*.

Agüera-Vega, F., Carvajal-Ramírez, F. & Martínez-Carricondo, P., 2017. Assessment of photogrammetric mapping accuracy based on variation ground control points number using unmanned aerial vehicle. *Measurement*, 98, pp.221–227.

Ali, Z., Tuladhar, A. & Zevenbergen, J., 2012. An integrated approach for updating cadastral maps in Pakistan using satellite remote sensing data. *International Journal of Applied Earth Observation and Geoinformation*, 18(1), pp.386–398.

Barnes, G. & Volkmann, W., 2015. High-Resolution Mapping with Unmanned Aerial Systems. *Surveying and Land Information Science*, 74(1), pp.5–13.

Bay, H. et al., 2008. {SURF}: Speeded up robust features. *Comput. Vis. Image. Und.*, 110(3), pp.346–359.

Bennett, R.M. & Alemie, B.K., 2015. Fit-for-purpose land administration: lessons from urban and rural Ethiopia. *Survey Review*.

Colomina, I. & Molina, P., 2014. Unmanned aerial systems for photogrammetry and remote sensing: A review. *ISPRS Journal of Photogrammetry and Remote Sensing*, 92, pp.79–97.

Crommelinck, S. et al., 2017. Contour detection for UAV-based cadastral mapping. *Remote Sensing*, 9(2), pp.1–13.

Devillers, R. et al., 2002. Spatial Data Quality: From Metadata to Quality Indicators and Contextual End-User Manual. *OEEPE/ISPRS Joint Workshop on Spatial Data Quality Management*, (March 2002), pp.45–55.

Devriendt, L. & Bonne, J., 2014. UAS mapping as an alternative for land surveying techniques? *International Archives of the Photogrammetry, Remote Sensing and Spatial Information Sciences - ISPRS Archives*, 40(3W1), pp.39–45.

Eltner, A. et al., 2015. Image-based surface reconstruction in geomorphometry – merits, limits and developments of a promising tool for geoscientists. *Earth Surface Dynamics Discussions*, pp.1445–1508.

Enemark, S., 2004. Building Land Information Policies. *UN, FIG, PC IDEA Inter-regional Special Forum on The Building of Land Information Policies in the Americas*, (October), pp.1–20.

Enemark, S. et al., 2014. *Fit-For-Purpose Land Administration*, Available at: https://www.dropbox.com/s/49v7w5kp5qw385d/Figpub60.pdf?dl=0%5Cnhttp://www.fig.net/resources/publications/figpub/pub60/figpub60.asp.

Furukawa, Y. & Ponce, J., 2010. Accurate, Dense, and Robust Multi-View Stereopsis Yasutaka. In *IEEE transactions on pattern analysis and machine intelligence*. pp. 1362–1376.

Gerke, M. & Przybilla, H.J., 2016. Accuracy Analysis of Photogrammetric UAV Image Blocks : Influence of Onboard RTK-GNSS and Cross Flight Patterns. *Photogrammetrie - Fernerkundung - Geoinformation*, (1–2016), p.14.

Grant, B.G., 2017. UAV imagery analysis: challenges and opportunities. 10204(May 2017), Spie proceeding 2017.

Hirschmüller, H., 2005. Accurate and efficient stereo processing by semi-global matching and mutual information. *IEEE International Conference on Computer Vision and Pattern Recognition*, 2(2), pp.807–814.

Hutton, J. et al., 2008. Tight Integration of GNSS Post-processed Virtual Reference Station with Inertial Data for Increased Accuracy and Productivity of Airborne Mapping. *XXIst ISPRS Congress Technical Commission V*, pp.3–11.

ISO, 2013. ISO 19157: Geographic information-data quality.

James, M.R. et al., 2017. Optimising UAV topographic surveys processed with structure-from-motion: Ground control quality, quantity and bundle adjustment. *Geomorphology*, 280, pp.51–66.

Jóźków, G. & Toth, C., 2014. Georeferencing experiments with UAS imagery. *ISPRS Annals of Photogrammetry, Remote Sensing and Spatial Information Sciences*, II-1(November), pp.25–29.

Kraus, K., 2007. *Photogrammetry: geometry from images and laser scans* 2nd editio., de Gruyter.

Lemmen, C. & Zevenbergen, J., 2009. First Experiences with High-Resolution Imagery-Based Adjudication Approach in Ethiopia.

Lowe, D.G., 1999. Object recognition from local scale-invariant features. *Proceedings of the Seventh IEEE International Conference on Computer Vision*, 2([8), pp.1150–1157.

Nex, F. et al., 2015. ISPRS Benchmark for Multi-Platform Photogrammetry. *Annals of Photogrammetry, Remote Sensing and Spatial Information Sciences*, II-3/W4(March), pp.25–27.

Nex, F. & Remondino, F., 2014. UAV for 3D mapping applications: A review. *Applied Geomatics*, 6(1), pp.1–15.

Orych, A., 2015. Review of methods for determining the spatial resolution of UAV sensors. *International Archives of the Photogrammetry, Remote Sensing and Spatial Information Sciences - ISPRS Archives*, 40(1W4), pp.391–395.

Pipino, L.L., Lee, Y.W. & Wang, R.Y., 2002. Data quality assessment. *Communications of the ACM*, 45(4), p.211.

Rahmatizadeh, S. et al., 2018. A framework for selecting a fit-for-purpose data collection method in land administration. *Land Use Policy*, 70(November 2017), pp.162–171.

Rahmatizadeh, S., 2018. Land Use Policy A framework for selecting a fi t-for-purpose data collection method in land administration. *Land Use Policy*, 70(October 2017), pp.162–171.

RCAA, 2016. *Ministerial Regulations No 01/MOS/Trans/016 of 26/04/2016 Relating to Unmanned Civil Aircraft System*,

Rehak, M., Mabillard, R. & Skaloud, J., 2013. a Micro-Uav With the Capability of Direct Georeferencing. *International Archives of Photogrammetry and Remote Sensing, Beijing, China*, XL(September), pp.4–6.

Remondino, F. & Pizzo, S. Del, 2012. Low-cost and open-source solutions for automated image orientation–a critical overview. *Progress in Cultural …*, pp.40–54.

Riza Nasrullah, A., 2016. Systematic Analysis of Unmanned Aerial Vehicle (UAV) Derived Product Quality. Master thesis. University of Twente.

Rosnell, T. & Honkavaara, E., 2012. Point cloud generation from aerial image data acquired by a quadrocopter type micro unmanned aerial vehicle and a digital still camera. *Sensors*, 12(1), pp.453–480.

Scherzinger, B. & Hutton, J., Applanix IN-Fusion TM Technology Explained. , pp.1–4.

Tonkin, T.N. & Midgley, N.G., 2016. *Ground-Control Networks for Image Based Surface Reconstruction : An Investigation of Optimum Survey Designs Using UAV Derived Imagery and*,

Toth, C. & Jóźków, G., 2016. Remote sensing platforms and sensors: A survey. *ISPRS Journal of Photogrammetry and Remote Sensing*, 115, pp.22–36.

Ullman, S., 1976. The interpretation of structure from motion. , (1), pp.1–5.

Zevenbergen, J. et al., 2013. Pro-poor land administration: Principles for recording the land rights of the underrepresented. *Land Use Policy*, 31, pp.595–604.

Appendix: Overview of UAV flights

All UAV images, intermediate results and final orthomosaics are stored on the share4land server (share4land.itc.utwente.nl:5566) with folder for each country and subfolder for each flight mission (see Fig. 33).

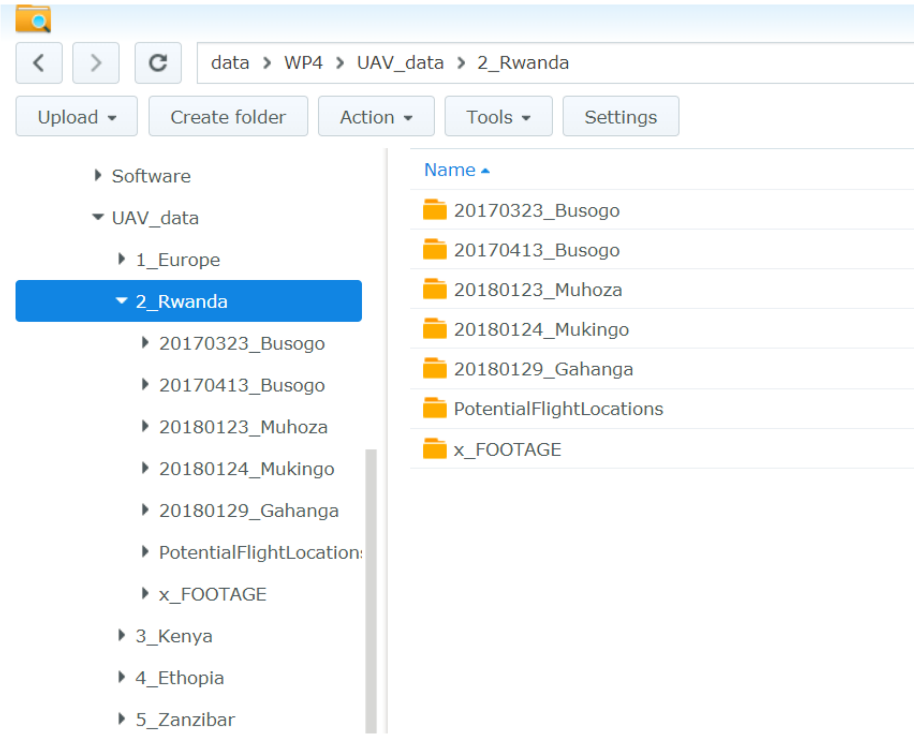

Figure 33: Folder structure on share4land Server

Each subfolder contains the raw images, ground control measurements and respective Pix4D projects named with the ID as mentioned in Table 13. Generated orthomosaics and digital surface models can be found in the folder 6_results. Additionally, all Pix4D quality reports are stored separately: /data/WP4/UAV_data/0_Pix4D_QualityReports

Table 13: Overview and specifications of all UAV datasets being used for this Deliverable.

Name (ID)	Date	Place	Area [km^2]	UAV	Camera	Images	GSD [cm]	Geotag	Overlap (f/s) [%]	GCPs	Check points
GER 1	Jul-16	Amtsvenn	2.09	GerMAP	Ricoh GR	662	4.86	No	80/65	5	8
GER 2	Mar-17	Coesfeld	1.4	DT18 PPK	DT18 RGB	2441	2.8	No	80/70	18	4
GER 3	Mar-17	Coesfeld	1.4	DT18 PPK	DT18 RGB	2441	2.8	PPK	80/70	4	18
GER 4	Mar-17	Coesfeld	1.4	DT18 PPK	DT18 RGB	2441	2.8	PPK	80/70	0	22
KE 1	Mar-18	Mailua	3.32	DT18 PPK	DT18 RGB	4421	5.72	Yes	80/70	4	3
KE 2	Mar-18	Mailua	3.32	DT18 PPK	DT18 RGB	4421	5.72	Yes	80/70	0	7
RW 1	Mar-17	Busogo	0.06	3DR Iris+	Canon Power SX 260 HS	141	2.18	No	80/70	9	4
RW 2	Mar-17	Busogo	0.06	3DR Iris+	Canon Power SX 260 HS	141	2.18	Yes	80/70	9	4
RW 3	Mar-17	Busogo	0.06	3DR Iris+	Canon Power SX 260 HS	141	2.17	Yes	80/70	0	13
RW 4	Jan-18	Busogo	0.54	Inspire2	Zenmuse Z5S	497	2.17	Yes	70/70	9	10
RW 5	Jan-18	Muhoza	0.98	FireFly	SONY A6000	991	2.16	Yes	70/70	9	20
RW 6	Jan-18	Muhoza	0.98	FireFly	SONY A6000	732	2.16	No	70/70	4	25
RW 7	Jan-18	Muhoza	0.98	FireFly	SONY A6000	991	2.16	Yes	70/70	4	25
RW 8	Jan-18	Muhoza	0.98	FireFly	SONY A6000	991	2.16	Yes	70/70	0	29
RW 9	Jan-18	Gahanga	0.14	DT18 PPK	DT18 RGB	372	2.62	Yes	80/70	9	5
RW 10	Jan-18	Gahanga	0.14	DT18 PPK	DT18 RGB	372	2.62	Yes	80/70	0	14
RW 11	Jan-18	Gahanga	0.14	DT18 PPK	DT18 RGB	372	2.62	No	80/70	9	5
RW 12	Jan-18	Busogo	0.54	Inspire2	Zenmuse Z5S	497	2.17	Yes	70/70	4	15
RW 13	Jan-18	Busogo	0.54	Inspire2	Zenmuse Z5S	380	2.17	No	70/70	4	15
RW 14	Jan-18	Busogo	0.54	Inspire2	Zenmuse Z5S	495	2.17	Yes	70/70	0	19
ZAN 01	Feb-18	Kibonde Muzungu	0.36	Ebee Plus	S.O.D.A	229	3.00	PPK	75/60	0	11
ZAN 02	Feb-18	Kibonde Muzungu	0.36	Ebee Plus	S.O.D.A	199	3.00	Yes	75/60	0	11
ZAN 03	Feb-18	Kibonde Muzungu	0.36	Ebee Plus	S.O.D.A	229	3.00	PPK	75/70	4	7
ZAN 04	Feb-18	Kibonde Muzungu	0.36	Ebee plus	S.O.D.A	229	3.00	No	75/60	6	5
ZAN 05	Feb-18	Kibonde Muzungu	0.36	Ebee Plus	S.O.D.A	229	3.00	PPK	75/60	4	7
ZAN 06	Feb-18	Kibonde Muzungu	0.36	Ebee Plus	S.O.D.A	229	3.00	No	75/60	4	7

Name (ID)	Date	Place	Area [km²]	UAV	Camera	Images	GSD [cm]	Geotag	Overlap (f/s) [%]	GCPs	Check points
ZAN 07	Feb-18	Kibonde Muzungu	0.36	Ebee Plus	S.O.D.A	360	3.00	PPK	75/80	0	11
ZAN 08	Feb-18	Kibonde Muzungu	0.36	Ebee Plus	S.O.D.A	360	3.00	PPK	75/80	4	7
ZAN 09	Feb-18	Kibonde Muzungu	0.36	Ebee Plus	S.O.D.A	267	3.00	PPK	75/70	0	11
ZAN 10	Feb-18	Kibonde Muzungu	0.36	Ebee Plus	S.O.D.A	360	3.00	No	75/80	4	7
ZAN 11	Feb-18	Kibonde Muzungu	0.36	Ebee Plus	S.O.D.A	267	3.00	No	75/70	4	7
ZAN 12	Feb-18	Kibonde Muzungu	0.7	Ebee Plus	S.O.D.A	87	7.00	PPK	75/70	0	11
ZAN 13	Feb-18	Kibonde Muzungu	0.7	Ebee Plus	S.O.D.A	87	7.00	PPK	75/70	4	7
ZAN 14	Feb-18	Kibonde Muzungu	0.7	Ebee Plus	S.O.D.A	88	7.00	No	75/70	4	7
ZAN 15	Feb-18	Kibonde Muzungu	0.53	Ebee Plus	S.O.D.A	144	5.00	PPK	75/70	0	11
ZAN 16	Feb-18	Kibonde Muzungu	0.53	Ebee Plus	S.O.D.A	144	5.00	PPK	75/70	4	7
ZAN 17	Feb-18	Kibonde Muzungu	0.53	Ebee Plus	S.O.D.A	144	5.00	No	75/70	4	7
ZAN 18	Feb-18	Kibonde Muzungu	0.22	Ebee Plus	S.O.D.A	533	1.50	PPK	75/70	0	11
ZAN 19	Feb-18	Kibonde Muzungu	0.22	Ebee Plus	S.O.D.A	533	1.50	PPK	75/70	4	7
ZAN 20	Feb-18	Kibonde Muzungu	0.22	Ebee Plus	S.O.D.A	478	1.50	No	75/70	4	7